Rheological modelling approach to evaluate the lithosphere under the Labrador basin (Offshore Canada).

Master's Project

Supervisors: Dr. Mohamed Gouiza and Dr. Charlotte. Botter

University of Leeds

by

Achyut Sankhe

201194668

ee17a3s@leeds.ac.uk

+44 7459207439

(Word court: 9320)

16/08/2018

Abstract:

The Labrador margin presents a transition from non-volcanic crustal characteristics in the south to volcanic crustal characteristics in the north. This is hypothesized to be the effect of laterally variable lithospheric strength across the Labrador Margin. Lithospheric strength can be measured by the upper rigid part of the lithosphere whose thickness is known as Effective elastic thickness (EET). EET is measured via an iterative modelling process that involves constraining the lithosphere thickness/ structure via integrated thermodynamic, geophysical and rheological modelling. The structure of the lithosphere within the basin is quite uncertain due to uncertainty in LAB depth. It can be better constrained through more iterations of the integrated modelling process and by taking the lateral variability of mechanical and thermal properties of the various rifted margins into account. Using a primitive lithosphere structure that is constrained by onshore surface heat flow calculations and minimal offshore residual mismatch, a principal model is produced to calculate laterally variable EET in the study area. EET maps over the study area show very low EET (<30km) within the basin itself. The decrease in EET is correlated to high loads. Even though a 3D geotherm is defined for the study area, the use of mono-compositional crust adds high uncertainty to the results. Important geological processes such as mechanical decoupling are overlooked in this modelling process causing the EET to be mainly constrained by the load. Further iterations of the proposed modelling process are required to take decoupling and 3D variation in crustal composition into account to get better constrained models of the study area.

UNIVERSITY OF LEEDS

SCHOOL OF EARTH SCIENCES

DECLARATION OF ACADEMIC INTEGRITY

To be attached to any essay, Dissertation, or project work submitted for assessment as part of a University examination.

I have read the University regulations on Cheating and Plagiarism, and I state that this piece of work is my own, and it does not contain any unacknowledged work from any other sources.

Name Achyut Ajay Sankhe

Signed _____

Date _____

Programme of Study

MSc Structural Geology with Geophysics

Acknowledgements

Primarily I would like to thank my supervisors Dr. Mohamed Gouiza and Dr. Charlotte Botter for giving me the opportunity to undertake a project that not only interests me but also will allow me to understand the field of Earth Sciences in a much broader way. I would also like to express my gratitude to Ben Craven and Dr. Charlotte Botter for being so supportive and providing IT help at times when I was completely stuck.

I am also grateful to the School of Earth and Environment at the University of Leeds that provided all the necessary tools (especially software) to tackle such a project. Thank you Dr. Gouiza for providing the necessary data required for the project and for being patient with me during times of delay and difficulty.

Also a sincere thank you to all the faculty and staff involved with MSc Structural Geology with Geophysics programme, especially Dr. Taija Torvela, Dr. Emma Brahmam, Dr. Douglas Paton and Amicia Lee for guiding and teaching me throughout the academic year.

Table of Contents

1 Introduction:

Rifted margins have been classified using two end member models:

- Volcanic rifted margins - form due to extrusive syn-magmatic events occurring alongside extension.
- Non-volcanic rifted margins - represent wide domains of extended crust with limited magmatism (Franke, 2013).

The differences between the two are the timing and extent of mantle melting in relation to lithosphere extension which in turn control the crustal architecture of rifted margins (Geoffroy et al., 2015).

In general, the crustal architecture of rifted margins can be divided as follows:

- Continental crust domain (CD)
- Transition domain (TD)
- Oceanic crust domain (OD).

These can be defined across all rifted margins despite differences in structural styles, lithology and magmatic budget (Gouiza and Douglas, in prep). The CD shows a shift from faintly deformed crust in the proximal margin to highly deformed and hyperextended crust in the distal margin. Such deformation due to extension is controlled by high angle listric faults (Franke, 2013; Gouiza and Douglas, in prep). In case of magma poor extension (i.e. at non-volcanic margins), the proximal and distal margins are divided by a necking zone. This zone acts as a transition from the proximal to distal CD and accommodates the crustal thinning observed in this transition (e.g.: Mohn et al., 2012). As we go seaward of the CD, the transitional domain (TD) is encountered.

At non-volcanic margins the TD is where lithospheric mantle is exhumed. Field analogues and high resolution seismic data from various non-volcanic margins have been used to study and characterize TD at said margins (e.g. Masini et al., 2012; Mohn et al., 2012). Such studies suggest that said exhumation occurs due to the hyperextension in the distal CD. This hyperextension can be attributed to highly localized deformation in such areas driven by the loss of ductility in the lithosphere (Peron-Pinvidic and Manatchal, 2009). However, TDs in volcanic margins have not been properly defined yet; their characteristics are still debated. The models proposed so far confirm the presence of syn-rift extrusive volcanic flows, which reflect in seismic data through seaward dipping reflectors (SDRs) (e.g. Soto et al.,

2011; Gladczenko et al., 1997). Subsequent to TD, on the further distal side (i.e. seaward) of rifted margins OD is reached, although relatively thin for non-volcanic margins and comparably thicker in volcanic rifted margins (Franke, 2013) (Figure 1).

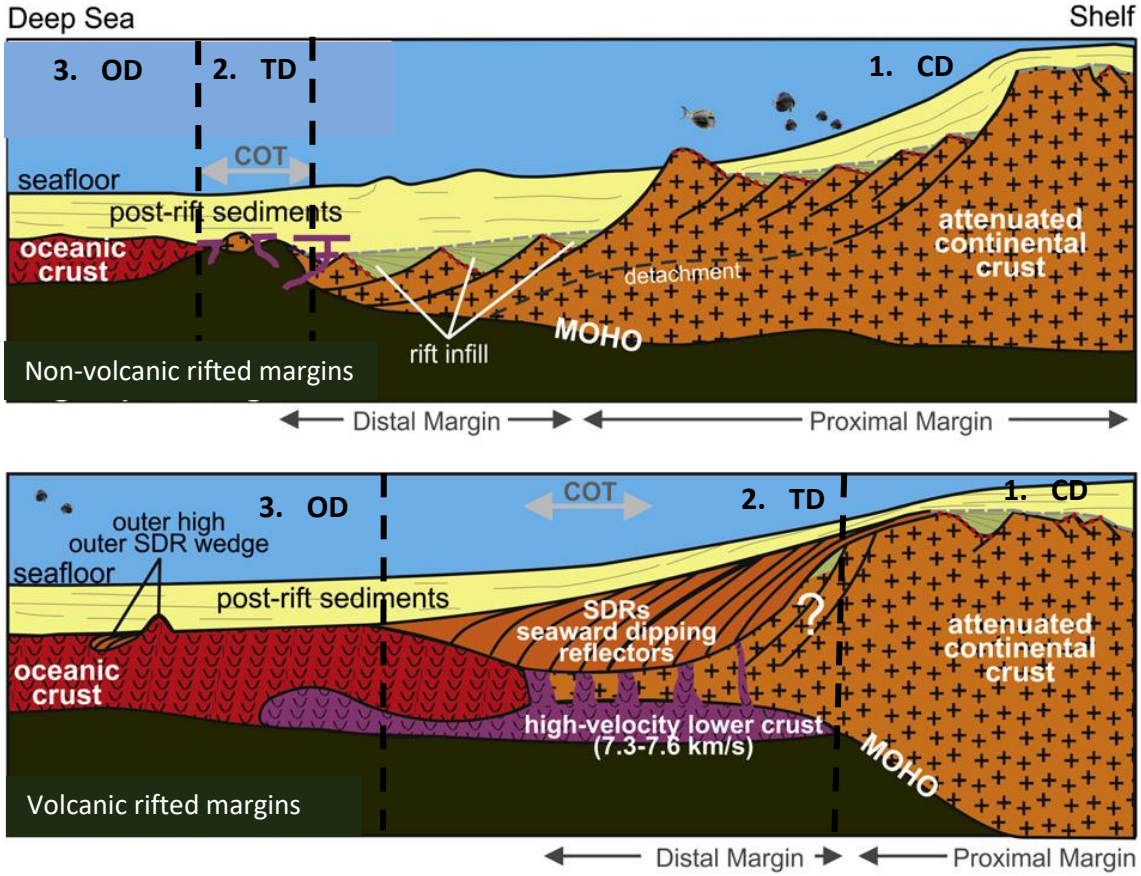

Figure 1: An illustration of end member rifted margin models and the different domain within them, courtesy of Franke (2013). COT refers to continent-ocean transition (a synonym for TD).

The Labrador- Newfoundland rifted margin presents a transition from non-volcanic to volcanic margin characteristics across the margin (Gouiza & Douglas, in prep; Dickie et al. 2011). The southern side of the Labrador margin represents what Franke (2013) defines as a non-volcanic rifted margin, whereas the northern side would be classified as volcanic rifted margin by Franke. This structural asymmetry across the margin is related to the variance in magmatic budget and lithospheric strength across it. (Gouiza & Douglas, in prep). This study attempts to understand this asymmetry by:

- understanding the crustal architecture across the Labrador basin/ margin
- detecting changes in lithospheric strength across the Labrador basin/ margin using rheological modelling and
- endeavouring to recognise the effect of laterally variable rheology of the lithosphere in controlling such asymmetry.

We use the integrated geophysical-petrological modelling method introduced by Alfonso (2008) and developed by Fullea et al. (2009) to model the lithosphere underlying the Labrador basin/ margin. We then apply the rheological module developed by Ros Bernarbeu (2013) based on work done by Burov & Diament (1995, 1996), Ventsel & Krauthammer (2001) to the developed lithosphere model so as to understand the impact of rheology on the structural evolution of the Labrador basin.

This study initially focuses on the fundamentals required to understand the motivation of this project. It then describes the geological setting of the region of interest (i.e. the Labrador basin). This is followed by the explanation of the data, methods and structural/ rheological modelling results. Finally, it also discusses the implications of obtained results and the scope of improvement for related studies in the future.

2 Fundamentals:

2.1 Rheology:

Rheology is the science of deformation - from how rocks deform under applied stresses to the study of the structures formed due to said behaviour. Initially, rocks deform elastically, but with the increase in the magnitude of stress and the time interval of their application; the rocks eventually reach their elastic limit (i.e. applied stress > yield stress of the rocks) at which point permanent brittle/ ductile deformation occurs leading to relaxation of elastic stresses.

- Brittle deformation refers to the loss of cohesion in the rocks due to the formation of fractures/ faults once yield stress is exceeded.
- Ductile deformation refers to plastic/ viscous flow (creep) of rock material once yield strength is exceeded.

Both rheological behaviours constitute ideal rheological models that describe the deformation of the lithosphere under tectonic stresses (Botter & Fullea, in prep.; Ros-Barnabeu, 2013; Burov & Diament, 1996).

Rheological behaviour within the lithosphere can be explained using constitutive rheological laws (e.g.: Turcotte & Schubert, 2002). Such constitutive laws are applied to build Yield strength envelopes (YSE). YSE are vertical profiles that indicate the variation of maximum differential stress supported by a rock with depth (Figure 2) (e.g.: Goetze and Evans, 1979). Temperature and pressure conditions at shallower levels drive the rocks to

brittlely deform – controlled by Byerlee's law. This law is independent of rock composition and gives the yield stress for brittle deformation based on pressure and friction. As we go deeper, the temperature increases and the rheological behaviour changes to ductile deformation. This rheological behaviour can be explained via a power law describing a dislocation creep. This law is mainly controlled by the temperature, strain rate and highly varies with rock composition (Botter & Fullea, in prep.; Ros Barnabeu, 2013). Therefore the variation of pressure, temperature and rock composition with depth are the main controlling factors of the transition of rheological behaviour in the lithosphere. Hence, when subjected to tectonic stresses the rheology of the lithosphere plays a major role in shaping the resultant structure.

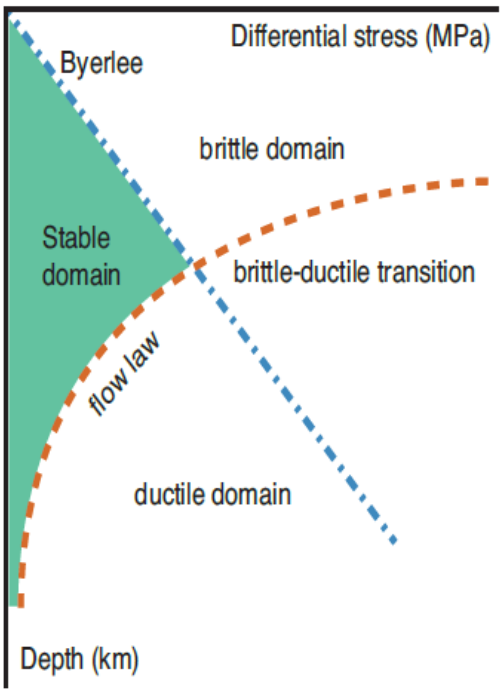

Figure 2: A schematic example of a yield strength envelope (YSE) showing the transition of rheological behaviour with depth and the laws controlling such behaviour. (Ros Bernabeu, 2013).

2.2 Lithosphere:

The lithosphere comprises the rigid outer shell of the Earth atop which sediments are deposited. It can be vertically divided into two broad layers: the crust and lithospheric mantle (Figure 3). The two layers are separated by the Mohorovičic discontinuity (Moho) which defines the compositional change from crust (predominantly mafic/ felsic) to the mantle (predominantly ultramafic). The 3D structure of these layers varies depending on location and its geological setting. For example: At rifted margins we observe a transition from thick to highly thinned crust as we go seaward due to a relative rise in the lithospheric mantle (i.e. necking of the lithosphere). The crust can be further divided into continental

and oceanic crust that form the aforementioned rifted margin domains CD and OD. The lithosphere also experiences temperature variations with depth, ending at its lower boundary which is considered an isotherm (surface of constant temperature: ca. 1600 K). These variations are controlled by the heat transfer mechanism of conduction and can be described using geotherms (Ros-Barnabeu, 2013). As mentioned before geotherms (i.e. temperature variation with depth) play an important role in defining the rheological behaviour of rocks in the lithosphere. Indeed, the 3D distribution of structure, temperature and composition in the lithosphere is what controls its rheology.

The lithosphere is also laterally divided into numerous plates that slide over the fluid like asthenosphere with relative ease. These plates are in relative motion with respect to each other controlling different structural features observed on the surface. For example: The diverging of two lithospheric plates leads to the formation of rifted margins and accretion of oceanic crust due to partial mantle melting . Such relative motion is a consequence of the ability of lithospheric plates to transmit elastic stresses over large distances and over geological time periods due to the inherent rigidity of the lithosphere. Rigidity also provides the property of flexure (bending) to the lithosphere when subjected to vertical topographic loads. Positive loads cause convex upward bending (e.g.: mountain chains) whereas negative loads cause convex downward bending (e.g.: sedimentary basins). Only the upper half of the lithosphere is rigid enough to not relax elastic stresses (i.e. transmit the elastic stresses/ avoid permanent deformation) on geological time scales. The thickness of this rigid fraction of the lithosphere is known as the effective elastic thickness (EET) (Turcotte & Schubert, 2002; Botter & Fullea, in prep.).

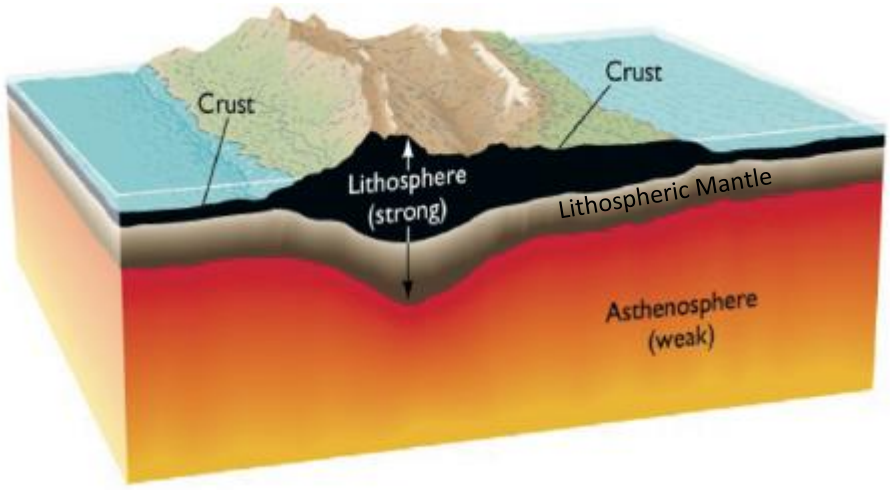

Figure 3: Cross-sectional view of the lithosphere (crust +lithospheric mantle) and asthenosphere. (Ros Bernabeu, 2013).

2.3 Effective Elastic Thickness (EET):

EET - the thickness of an imaginary elastic plate used to model the lithosphere that supports part or all of the topographic load (Burov & Diament, 1995, 1996). As mentioned above it is mainly controlled by the rigidity of the lithosphere and can be used as a proxy for lithospheric strength (Botter & Fullea, in prep.). Therefore, an accurate estimation of EET is crucial to understand the role of lithospheric strength in shaping present day geological structures that formed due to relative motion of lithospheric plates. EET can be divided into two components:

- flexural component
- structural component

The flexural component relates to the flexural response due to loading and can be determined based on isostatic principles. Isostasy refers to a compensation level at which large surface loads are balanced. The depth of such a level is dependent on EET. When dealing with local isostasy, EET = 0, i.e. the lithosphere has no rigidity (Airy-Pratt models: e.g.: Turcotte & Schubert, 2002). This requires the mass per unit area of the lithospheric columns to be equal at a certain compensation depth. However this is an unrealistic assumption that leads to unrealistic elevations and gravity anomalies (Fullea et al. 2009). Therefore the concept of regional isostatic compensation is applied where EET has a non-zero value and takes the deflection (flexure) of the lithosphere due to loading into account. Indeed, if the rigidity and therefore EET is too high (i.e. a stiff plate), there will be no flexure observed as the load is completely supported by the internal stresses of the lithosphere (Botter & Fullea, in prep.; Ros-Barnabeu, 2013). However, rifted margins and areas of recent tectonic activity are theorized to have relatively low EET values (<40km) (Audet & Bürgmann, 2011). Therefore, the last scenario is not applicable in this study.

EET is also defined by the 3D structure of the two lithospheric layers (crust and mantle) i.e. the structural component. It takes into account vertical composition, density, temperature distribution, strain rate, the fluid content and pore fluid pressure (Botter & Fullea, in prep.). Such properties define the rheology and hence rheological behaviour within the lithosphere. This behaviour within the lithosphere changes with depth as discussed in section 2.1. Indeed, the lithosphere is not a laterally homogeneous feature. The lateral variation of aforementioned properties and hence the rheology of the lithosphere causes 3D variation of rheological behaviour within the lithosphere. This 3D

variation must be taken into account when calculating for lithospheric strength via EET. Therefore, by calculating the 2D distribution of topographic load (through which flexure of the lithosphere is derived) and integrating it with 3D distribution of rheological properties (defined by the 3D variation of structure and lithology), both components of EET are accounted for. Through this an accurate estimation of laterally varying lithospheric strength i.e. EET can be made.

3 Regional Overview:

The Labrador basin is located offshore between Newfoundland and Greenland, towards the northern edge of the North Atlantic (Figure 4).

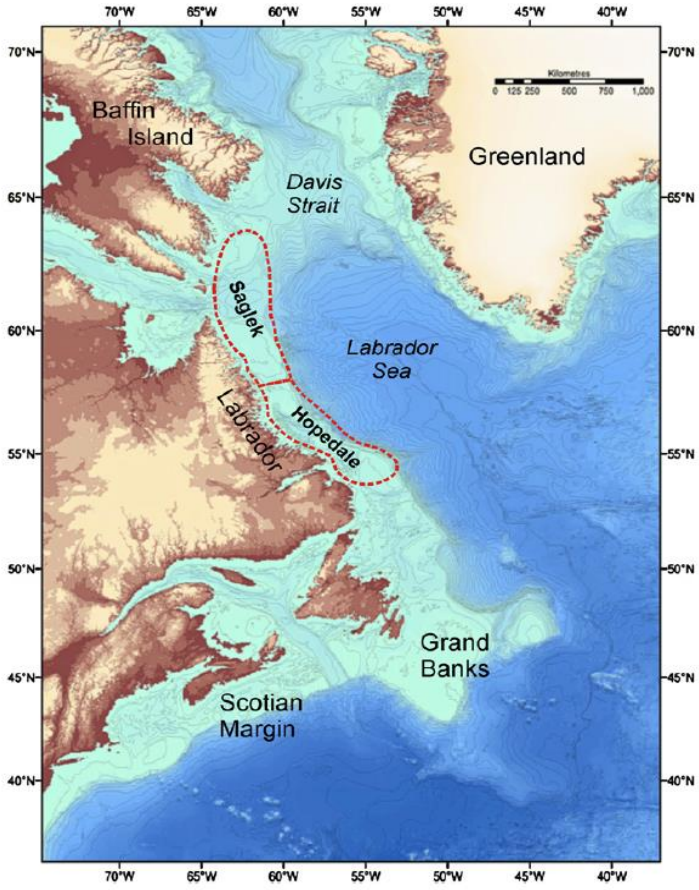

Figure 4: The location of the Labrador basin/ margin. The Hopedale basin approximately covers the southern area representing non-volcanic margin characteristics whereas the Saglek basin reflects volcanic margin characteristics (Section 1)

3.1 Geological History:

3.1.1 Pre-Rift Geological Setting:

The pre-rift basement is Palaeozoic, housing several pre-Mesozoic tectonic events is exposed onshore Labrador (Canada). It provides evidence that the Greenland and Labrador lithospheric plates were linked before the initiation of rifting which comes from 'temporal and compositional correlations' of Lamproites found in both areas

(Gouiza & Paton in prep; Tappe et al., 2007). It is divided into three 'tectonic units' starting from Archean Nain Province in the north to the Palaeoproterozoic Makkovik and Late Palaeoproterozoic Grenville Provinces towards the south (Gouiza & Paton, in prep). The Kanairiktok Shear zone separates the Nain from the Makkovvik province whereas the Grenville suture/ front separates the Greenville province from Makkovik. All provinces are mainly comprised of igneous and highly metamorphized rocks (e.g.: gneiss, granitic intrusions: Culshaw et al., 2000; Van Kranendonk et al.,1993; Gouiza & Paton, in prep) along with of a mixture of Paleozoic clastics and carbonates preserved on the south-western edge Labrador shelf (Dickie et al., 2011).

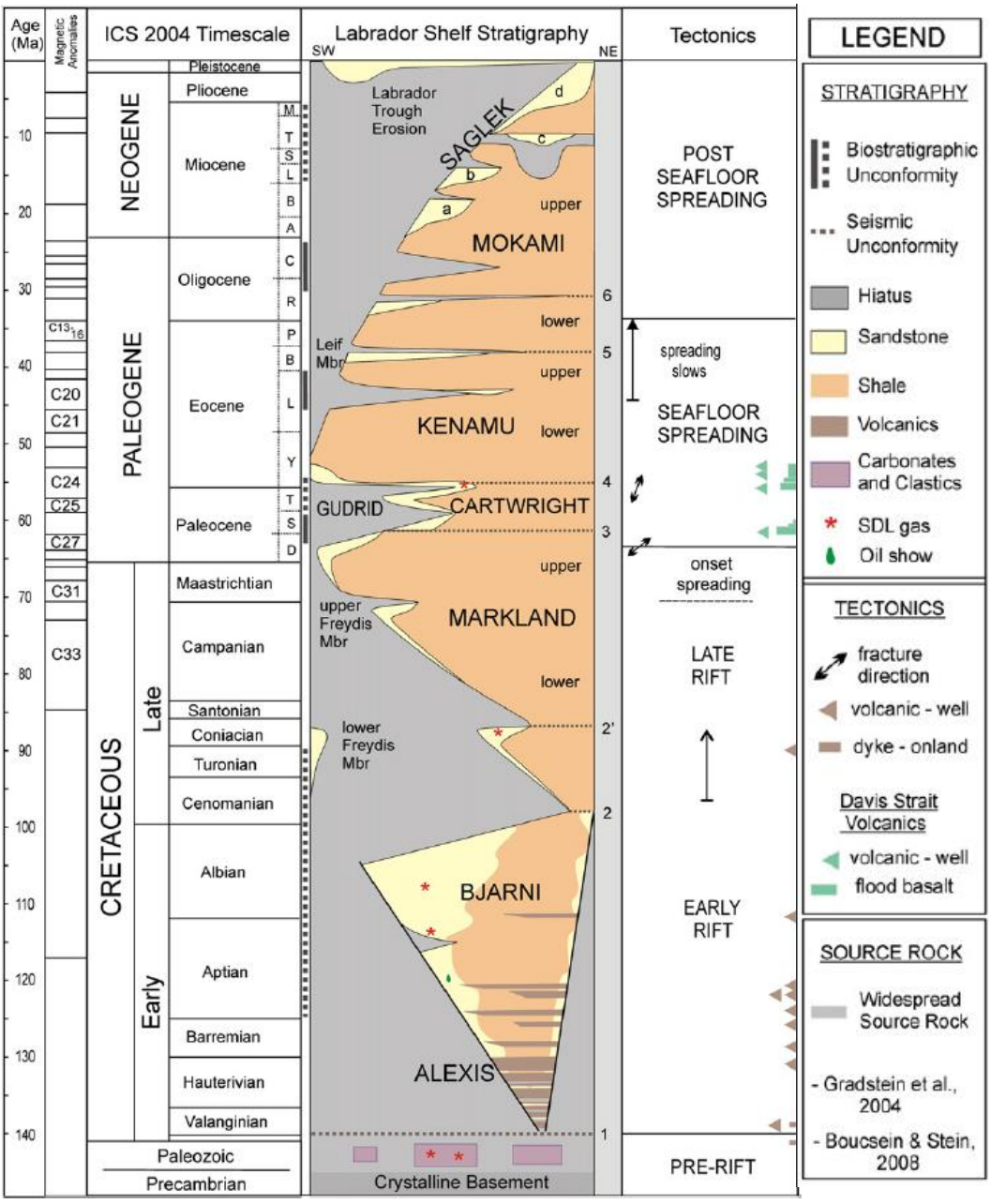

Figure 5: The tectonostratigraphic development of the Labrador margin relating various formations to the different phases of rifting (courtesy of Dickie et al., 2011).

3.1.2 Mesozoic Rifting:

Rifting in the North Atlantic commenced during Late Triassic- Early Jurassic separating Newfoundland and Iberia (Gouiza & Paton in prep). As rifting progressed, it shifted northwards and by Early Cretaceous SW Greenland and Labrador were being extended (Dickie et.al 2011). The accommodation space for syn -rift sediments was created by normal faults oriented NW-SE that generated graben/ half-graben geometries.

Dickie et al. (2011) suggest a two-phase rift history for Mesozoic rifting in the Labrador basin (Figure 5). Early rifting (ca. 140-100 Ma: Valanginian - Albian) caused extension and thinning across Labrador and Greenland shelves and late rifting (ca. 100 – 65 Ma: Cenomanian – Maastrichtian) happened offshore, away from the shelves in the distal margin. The latter was localized and responsible for mantle exhumation in parts of the Labrador margin.

3.1.3 Syn-Rift Basin fill:

During early rifting the accommodation space was filled by interbedded clastics and volcanics (e.g.: Alexis and Bjarni formations). These sediments were laterally variable, mainly comprised of a mixture of sand and shale units. As the late rift phase was reached there was a clear transition to deep marine systems as indicated by an increase in the shale content of the Late Cretaceous Markland formation (Figure 5). Localized rifting during this phase eventually lead to sea- floor spreading in the Palaeocene (ca. 65 Ma.).

3.1.4 Sea-floor spreading:

Gouiza & Paton (in prep) present a diachronous breakup mechanism based on the analysis of magnetic anomalies/ chrons. They suggest that the beginning of oceanic crust generation occurred between magnetic Chron 29 (ca. 65.8-64.4 Ma; Srivastava and Roest, 1999) and 27 (ca. 63.3-61.1 Ma; Roest and Srivastava, 1989) at the southern Labrador margin (Figure 4). Whereas at the northern margin initial accretion occurred around magnetic Chron 26 (ca. 60.5-57.7 Ma; Roest and Srivastava, 1989), suggesting that oceanic crust generation occurred later in the north versus in the south in the Labrador basin. However lot of debate still remains around the timing of initiation of seafloor spreading and the exact mechanism is still uncertain.

3.1.5 Post-Seafloor Spreading:

As seafloor spreading subsides there is a major unconformity observed in the stratigraphic column (at the top of the Markland formation: early Palaeocene ca. 60 Ma.: Figure 5) theorized to be the consequence of the arrival of a Proto-Icelandic plume in the Davis Strait region (north of the Labrador margin: Figure 4). This unconformity forms the base for the deposition of younger sediments (Palaeocene onwards). The clastic nature of the post-rift sediments is a product of the multiple relative sea-level transgression and regression phases. On a regional scale it can be inferred that these sediments are dominated by finer grained shaley sediments compared to the syn-rift sediments (Dickie et al., 2011).

3.2 Evidence of Asymmetry at the Labrador margin

3.2.1 Variance in TD:

Srivastava and Roest (1999) examined geophysical data (mainly seismic refraction) collected from the northern margins (around Saglek basin ~ 54°N – 60°N) of the Labrador Sea. Their conclusion was that although there is evidence of mantle unroofing (i.e. exhumed mantle: TD of non-volcanic margin), during slow seafloor spreading in the Labrador sea; the presence of a low velocity top crustal layer (4 – 5 km/s) (e.g.: Chian and Louden, 1995; Chian et al., 1995a) and symmetric magnetic anomalies corresponding to oceanic crust or highly deformed continental crust, indicate the unlikelihood of such mantle unroofing being active across the northern Labrador margin. Therefore the nature of TD can be considered to vary across the margin.

This variance is also evidence by TD seismic reflections as they change between southern to the northern Labrador margin. In the south the seismic reflectors are discontinuous with variable amplitude slowly transitioning into wedge like high amplitude reflectors dipping seaward (SDRs) towards the north (Gouiza & Paton, in prep).

3.2.2 Variance in Crustal Architecture:

On considering the overall crustal architecture, the southern margin is characterized by a narrow necking zone (ca. 25- 70 km) followed by a highly thinned and wide distal CD similar to observations from the Newfoundland/ Iberia margin. Therefore, a similar model can be applied to the southern Labrador margin that involves hyperextension in the distal parts of the CD and TD with the latter being characterized by exhumed serpentenized subcontinental mantle (Gouiza & Paton, in prep.; Peron-

Pinvidic and Manatchal, 2009; e.g.: Suckro et al., 2012) i.e. a magma poor extension model.

Contrastingly, the northern margin is branded by a wide necking zone (ca. 100 km) and no hyperextension in the distal CD. The northern margin is also highlighted by the presence of SDRs in this region signalling the presence of flood basalt wedges. These characteristics are more typical of magma rich margins as defined by Planke & Eldholm (1994) and Franke, (2013) (Gouiza & Paton, in prep.). The transition from magma poor and magma rich is not sudden and is marked by high amplitude reflectors in the distal CD and TD indicating volcanics (e.g.: dykes and sills) (Gouiza & Paton, in prep.).

3.2.3 Variance in Crustal properties:

Variability in other geophysical properties such as crustal thickness and surface heat flow across the Labrador margin also highlights asymmetry. Funck et al. (2001) reported a change in crustal thickness from the Makkovik (35 – 40 km) to Grenville (50 km) domain. Mareschal & Jaupart, (2004) collected onshore Labrador margin data that indicated a gradient in surface heat flow, increasing north to south. Considering the aforementioned three pre-rift provinces discussed in Section 3.1.1, it was found that surface heat flow in the Nain/ Churchill province ranged between 22—27 mW/m^2. The Makkovik and Grenville provinces showed a higher average with ranges of 27—37 mW/m^2 and 27—47 mW/m^2 respectively thus depicting higher surface heat flowing southward compared to the north (Gouiza & Paton, in prep.).

3.3 Effect of Lithospheric Strength

Given the evidence of the asymmetric nature of the Labrador margin, it is important to understand the factors influencing this asymmetry. Past studies of lithosphere extension have postulated lithospheric strength to play a major role in defining the nature of extension and hence structures observed due to such extension (e.g.: Huismans & Beaumont, 2003; Buck, 1991). Lithospheric strength is a consequence of the thermal structure and composition of the lithosphere (i.e. its rheology). Indeed, if those properties were variable across a region at the time of deformation, the way in which rocks across the region deformed will also vary. This will then have an impact on present day crustal structures and overall architecture (Gouiza & Paton, in prep.). Therefore lithospheric strength across the Labrador margin should be evaluated in order to gain insight into present day structural asymmetry and the temporal evolution of the Labrador margin.

As discussed in section 2.3, lithospheric strength can be estimated through EET. This requires one into take account both the topographic load acting on the lithosphere and its rheology. Previous studies have attempted to estimate EET by forward modelling approaches, but they do not factor the 3D variation in rheology (e.g.: Pérez-Gussinyé et al., 2005). Hence the lithospheric strength estimates by such processes are controlled mainly by the flexural effect of loading. This study attempts to integrate the 3D rheological variation effect into the Labrador basin to calculate laterally variable EET using an integrated thermodynamic, geophysical and rheological modelling approach.

4 Data and Methods:

The scope of this project includes the Labrador-Newfoundland margin and the Labrador Sea (Figure 6). The methodology for this project was tailored to produce a 3D rheological model representing laterally variable EET and can be divided into three major components: Seismic Interpretation, Integrated Geophysical- Petrological modelling and Applying the 3D rheological module. A summarized workflow is presented in Figure 7.

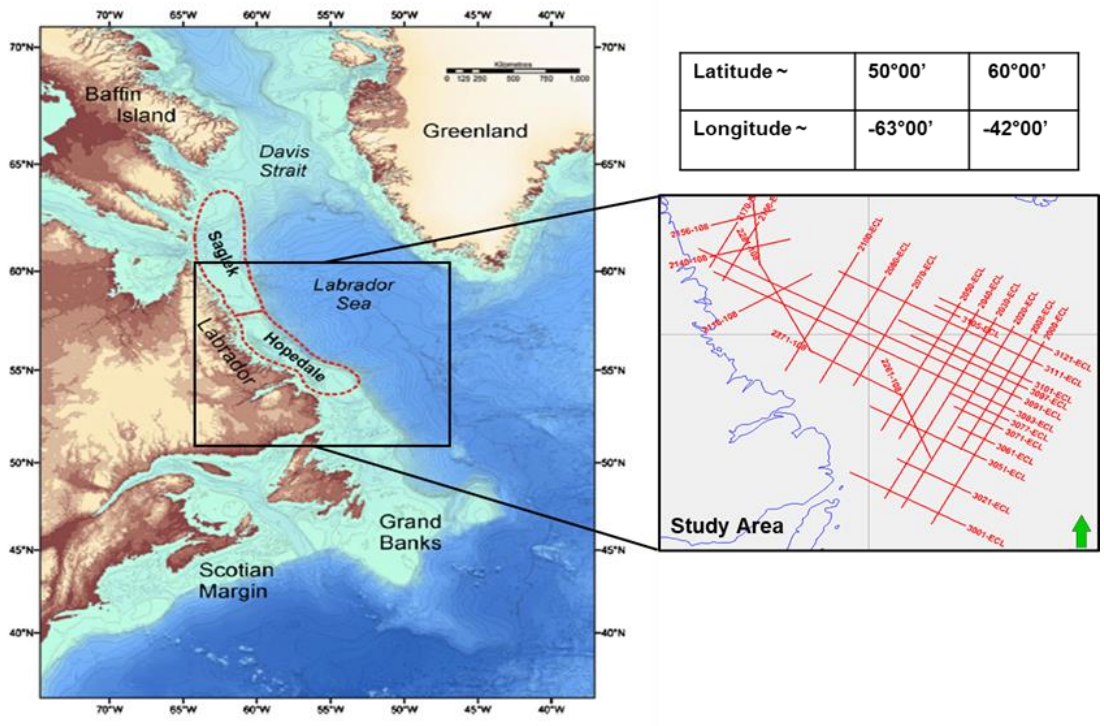

Figure 6: The extent of the study area for this project including the 2D regional seismic lines.

4.1 Seismic interpretation:

Seismic interpretation is carried out on Petrel using thirty-one regional seismic lines present offshore of the Labrador coast explored by TGS (Figure 6). Interpretation was driven by the established Labrador margin asymmetry (section 3.2). This step involves the interpretation of major surfaces and defining their geometry across the study area. These surfaces are used to constrain the models proposed in this study.

- Top Post-rift basin fill
- Top Syn-rift basin fill
- Top Pre-Rift basement
- Mohorovičić boundary
- Lithosphere-Asthenosphere boundary (LAB).

These surfaces were initially interpreted by Gouiza & Paton (in prep.). For this study the surfaces were reviewed and extended/ interpolated across the study area. Except LAB and Mohorovičić, all other surfaces were completely interpreted on the TGS 2D regional seismic lines. These surfaces were:

- Constrained with well data in the northern part of the study area and extrapolated across the seismic lines in the study area.
- Interpreted in time and were converted to depth contoured surfaces using the velocity model developed by Gouiza et al. (2017).

The Moho boundary was constrained by satellite free-air gravity data (Sandwell et al., 2014) and had to be revised based on its proposed position in the various domains of the end member rifted margin models (volcanic/ non-volcanic: section 1). The LAB surface is of utmost significance as it defines lithospheric thickness and thermal structure. Its interpretation is iterative based on a feedback process. This is discussed later in detail in section (5.2). These surfaces defined 4 layers in the study area that include

- Post-rift fill
- Syn-rift fill
- Pre-rift Crust
- Lithospheric mantle.

The geometries of these layers are then used as input variables for the next step i.e. Integrated Geophysical-Petrological modelling.

4.2 Integrated Geophysical-Petrological Modelling

This step is essentially a quality control stage to verify the structure and composition of the lithosphere underneath the study area. This is done via *LitMod3D*, a software used for modelling the lithosphere and sub-lithospheric mantle based on thermal, compositional, density, seismological, and rheological properties (Fullea et al. 2009). The modelling process outputs calculated geophysicals which are compared and fitted to observable geophysicals in order to obtain an accurate structural and property model of the lithosphere.

LitMod3D: The software is based on a collection of FORTRAN sub-routines and shell scripts, divided into two modules: *LITMOD3D_FOR*, a forward calculation module and *LITMOD3D_INTF*, a graphical interactive interface to visualize and adjust the produced models. The former outputs calculated variables, while the latter helps visualize the 3D structure of the study area and provides a platform to compare calculated output and observable data. Another essential part of the software is a shell script: *LITMOD_3D.job* that centralizes input data and generates the input files used by the two predefined modules for calculations/ visualization of the model (Fullea et al., 2009).

Input: The major input variables required for the calculation of output geophysicals and structural model construction are layer geometry/ composition and an initial EET value. Layer geometry in 3D is defined via seismic interpretation as each layer is demarcated by the aforementioned surfaces. EET is assumed to be 40km which is considered a reasonable estimatefor a geologically young rifted margin (E.g.: Botter et al., 2017).

Compositional variables for the layers mainly include density and thermal parameters. The main sources used to assign these parameters include Gouiza & Paton (in prep.), Botter et al. (2017) and Eugene (1988). The bottommost layer i.e. the sub-lithospheric mantle has pre-defined compositional files from LitMod3D. The Lherzolite file was used during this project. LitMod3D uses these input parameters to solve heat transfer, thermodynamic, geopotential, isostasy and flexure equations (Fullea et al., 2009; Afonso et al., 2008; Botter & Fullea, in prep.)

Output: Based on the aforementioned calculations the software outputs temperature distribution (3D lithospheric geotherm), density, lithostatic pressure, heatflow, gravity anomalies, geoids, and flexural and isostatic elevations along with a structural model based on the layer geometry provided. The calculation methods (equations) of the forward module for these parameters as well as visualization

controls for the produced integrated model are explained in detail by Fullea et al. (2009) and Botter & Fullea (in prep.).

Comparison: The output calculated variables used for comparison with observed data include the gravity anomalies, heat flow and local isostatic/ flexural elevation. The observed elevation and gravity anomalies (Bouguer and Free Air Anomaly) were determined from public domain topography and gravity data (Smith & Sandwell, 1997; Sandwell et al., 2014) whereas Geoid and Bouguer were derived using NGA public domain data. Heatflow data values were used from Mareschal & Jaupart (2004). The comparison was done via LitMod3D generated residual maps that highlighted the difference between the calculated and observable data. When comparing the calculated and observable variables, the focus was to rectify mismatches by adjusting input variables (layer geometry and composition) so that the regional trend of calculated variables matched the regional trend of the geophysical observables (Botter & Fullea, in prep.). Once this criteria was met, layer geometry and composition was considered verified (to some extent) and the structural/ property model (based on layer geometry/ composition) accuracy was considered acceptable. We then applied the 3D rheological module to such a model in order to calculate laterally variable EET.

4.3 Apply 3D Rheological Module:

The 3D integrated geophysical-petrological model is built on a 3D grid. The rheological module calculates effective elastic thickness (EET) for each column of this grid.

Input: There are two major input categories for the rheological module: User input and LitMod3D calculated outputs. User input includes defining an initial constant value of EET, strain rate, Poisson ratio, Young's modulus along with rheological law parameters (brittle and ductile: section 2.1). LitMod3D outputs used for the rheological module include topographic load (derived from the pressure difference at the base of the each column of the grid during the calculation local isostatic elevation), temperature distribution and density (Botter & Fullea, in prep.). The load aids the calculation of the flexural component of EET and the rest of the input parameters help compute the structural component (section 2.3).

Calculations: The module calculates EET via a main iteration loop. The initial value of EET is required at the start of the loop as it provides a rigidity value that is necessary to compute deflection (flexure). This constant EET value was also input during the LitMod3D modelling process too. It converts to a laterally variable value by integrating the effect of variable lithospheric strength (i.e. variable rheology) and

topographic load during the first iteration of the main loop. The laterally variable EET becomes the input for the subsequent iteration.

The subsequent iterations follow a similar process. They begin with the calculation of deflection which is the first step followed by the calculations of bending curvature and elastic strength. The next step involves calculating finale strength by integrating the effect of rheology, followed by bending moment and rigidity computations. The rigidity values are then used to define EET across the study area. Running the loop is an iterative process and is done to until EET values stabilize (Botter & Fullea, in prep.).

Output: By applying the 3D rheological module, we get two main outputs: Load and EET. The load of the lithosphere pertain to the flexural component of EET. The load should match the difference between local isostatic and observed elevation from LitMod3D as the mismatch in that comparison should be compensated for by the flexural effect of topographic loading. The EET output takes both components (structural and flexural) into account and highlights the overall lithospheric strength. More importantly it could highlight the effects of varying rheology on lithospheric strength across the study area (Botter et al., 2017; Botter & Fullea, in prep.).

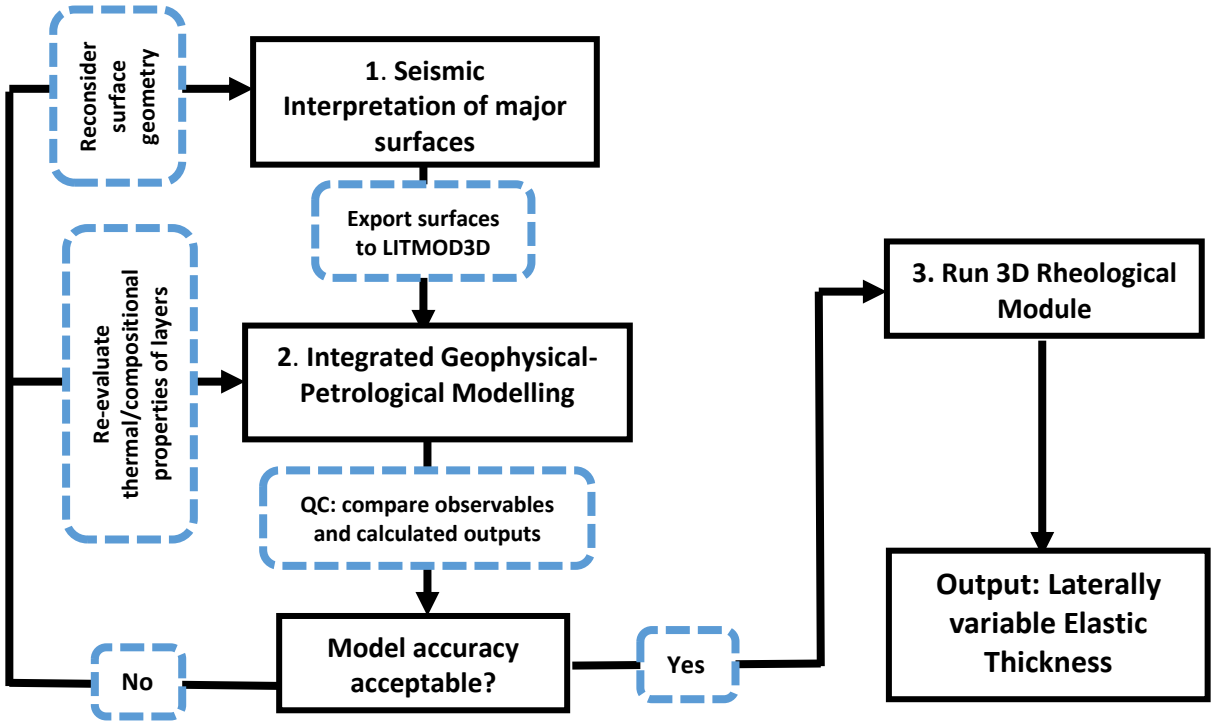

Figure 7: A summarized workflow diagram showing the three steps involved to produce a laterally variable EET map of the study area.

5 Data Interpretation

Based on the presented methodology, data interpretation can be divided into 3 stages: (1) Defining the structural/ property model, (2) Verifying via geophysical-petrological modelling and (3) Generating an EET map of the study area.

5.1 Defining structural/ property model:

Seismic interpretation provided insight into the main structures controlling the layer geometry and the variation of margin geometry from north to south.

5.1.2 Layer Geometry:

Layer 1 - Post- Rift deposits: The layer is bound by *Top Post-rift basin fill* at the top and *Top Syn-rift basin fill* at the bottom and follows a thickness trend as we go from north to south. Depocenters for this layer are spread over the continental shelf, slope and the deep distal margin in the north, whereas in the south they are located in the deep distal margin (i.e. seaward of the continental slope) for the most part evidenced by the layer thinning out as we approach the continental shelf (Figure 8,9). The layer also has been assumed to pinchout before reaching the onshore margin as we know that pre-rift basement is exposed onshore Labrador margin (Gouiza & Paton, in prep.).

Layer 2 – Syn- Rift deposits: Delimited by the *Top Syn-rift basin fill* at the top and *Top Pre-Rift basement* at the bottom this layer has depocenters seaward of the continental slope across the whole study area. The seaward of slope represents the distal part of the CD and is marked by numerous northeast/ southwest dipping listric normal faults cutting through the basement (bottom extent) that are theorized to form as a result of localized extension during latter part of rifting (section 3.1.2 e.g.: Mohn et al., 2012; Gouiza & Paton, in prep.). These faults created the main accommodation space for syn- rift deposits thus forming depocenters. Towards the south this area of localized faulting is quite wide (Figure 8). It gets narrower in seismic lines present north of the Cartwright fracture zone (CFZ) (an important shear structure that accommodated change in extension nature during rifting; defined by Gouiza & Paton, in prep.) (Figure 9, 10). Only a few faults exist on the shelf and slope resulting in very little accommodation space for syn-rift deposits. The syn-rift deposits pinchout towards the northeast due to accretion of oceanic crust during the sea-floor spreading phase (section 3.1.4). They are also considered to pinchout southwest due to aforementioned onshore basement exposure (Figure 8, 9).

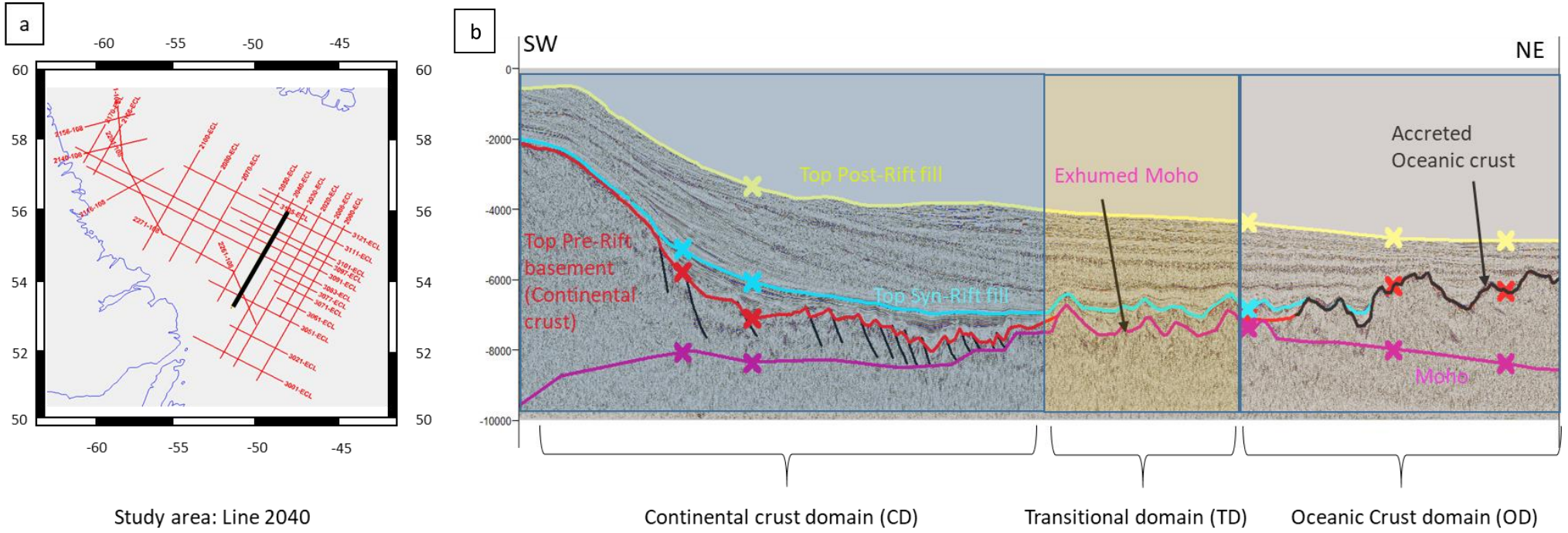

Figure 8: (a) The orientation of seismic lines (used for surface interpretation) in the study area highlighting crossline 2040-ECL. (b) The interpretation of surfaces (except LAB) on the highlighted seismic line (vertically exaggerated) showing the three different domains of the rifted margin. Southern Labrador margin shows a mantle exhumed TD.

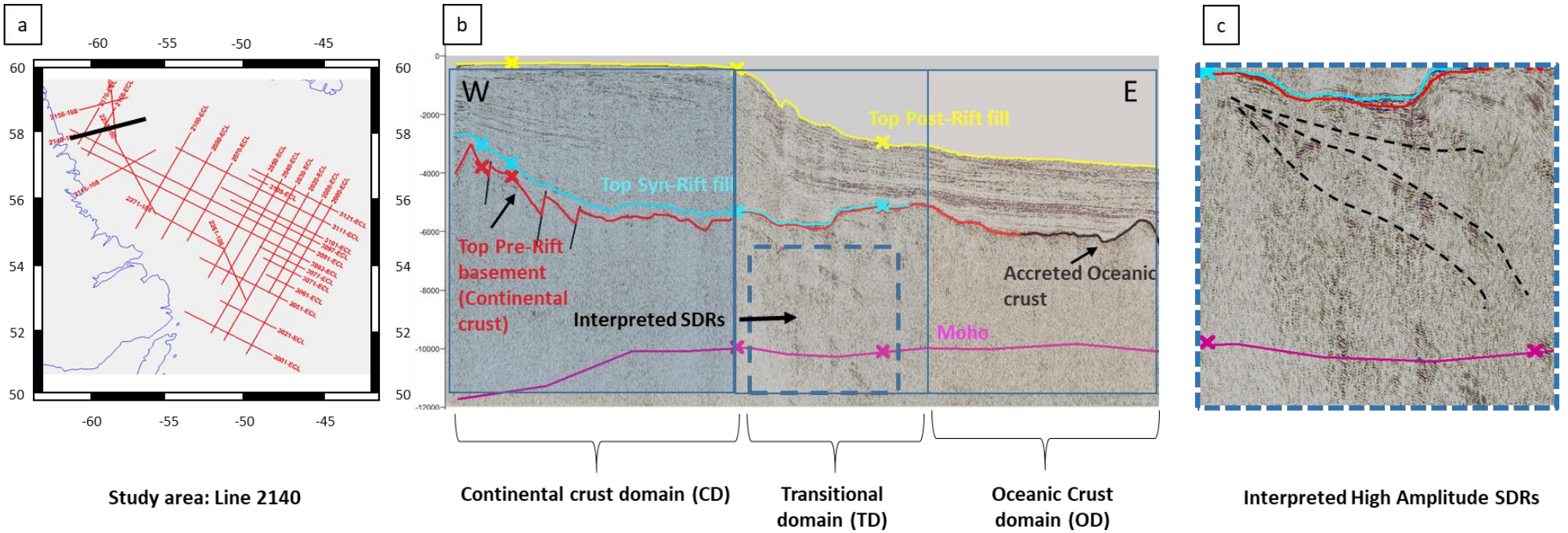

Figure 10: (a) Study area seismic lines with highlighted line 2140-108. (b) Interpretation of surfaces (except LAB) on the highlighted line (vertically exaggerated) showing the three different domains of the rifted margin. (c) A close look at the TD towards the northern side of Labrador shows high amplitude seaward dipping reflectors (SDRs).

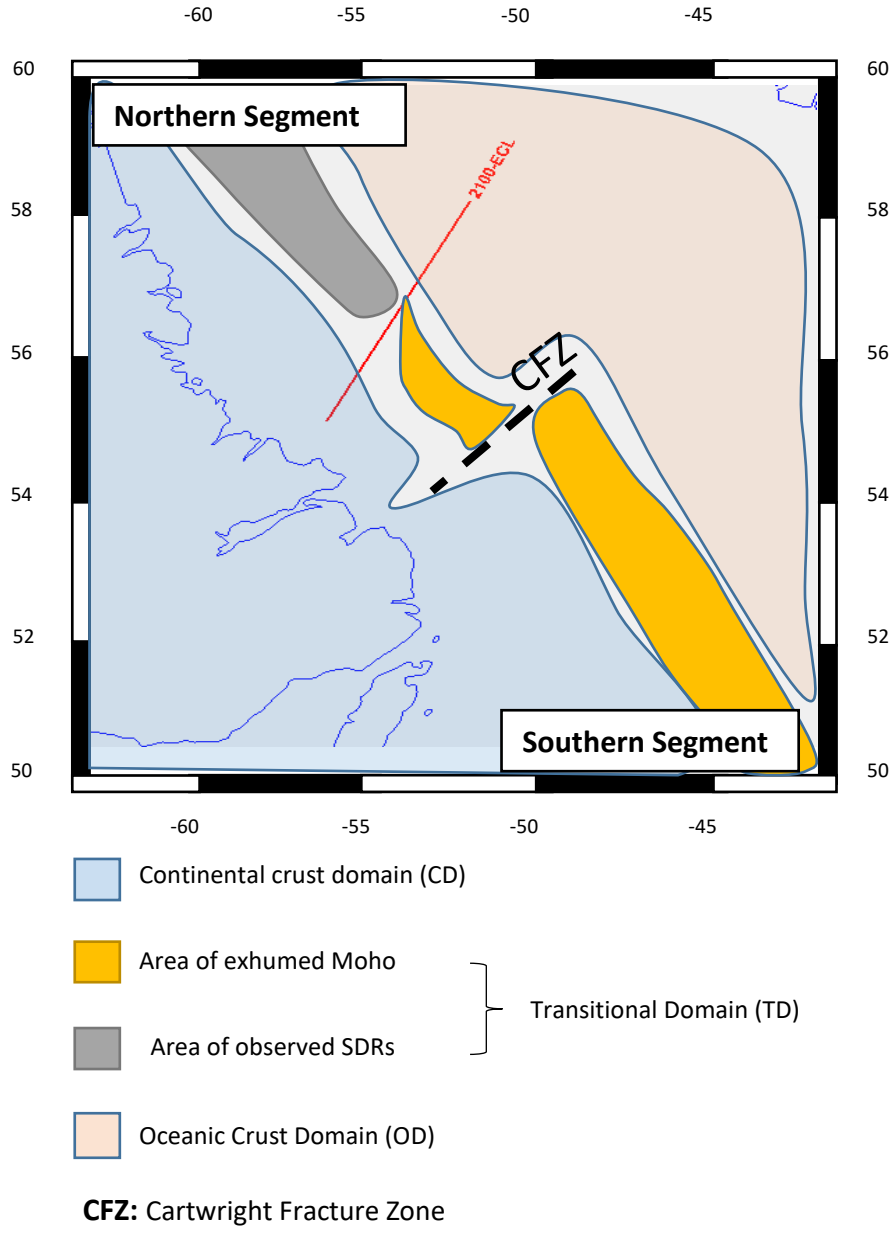

Figure 10: The different rifted margin domains observed in the study area along with the division of the study area into northern and southern segments based on variance in TD and crustal architecture characteristic.

Layer 3 – Pre- Rift/ Oceanic crust: This layer marks the beginning of the lithosphere and represents crustal architecture. It is marked by aforementioned normal listric faults cutting across the *Top Pre-Rift basement* which defines the upper extent of this layer. The lower extent of this layer is marked by *Mohorovičić boundary* (Moho). In the southern segment layer 3 has no thickness in some extents due to Moho being exposed on top of the basement in those areas (i.e. mantle exhumation). These extents define the TD of non-volcanic southern Labrador margin (Figure 8). The TD in this segment is also displaced by the CFZ shifting the TD towards the west on the northern side of CFZ. Contrastingly, layer 3 has non-zero thickness throughout the northern segment and is marked by the presence

of SDRs (Figure 9). Further variance in crustal architecture has been highlighted in section 3.2.2.

Study Area Segments: Based on the structural variance of the aforementioned three layers, the study area can be divided into two segments. Based on TD characteristics the study area was understood to transition from non-volcanic margin to volcanic margin characteristics around crossline 2100-ECL (Figure 10) based on seismic reflection character highlighted by Gouiza & Paton (in prep.) and as observed during seismic interpretation (Figures 8, 9). Therefore this line was used as a marker to divide the study area into two segments: (1) northern segment (north of line 2100-ECL) and (2) southern segment (south of line 2100-ECL).

Layer 4 –Lithospheric Mantle: The upper bound of this layer is the Moho - details are discussed in the previous section. The lower bound of this layer is the *Lithosphere-Asthenosphere boundary* (LAB). LAB marks the end of the lithosphere. Thus *Layer 4* and *Layer 3* together define lithospheric thickness in the study area. However, seismic data is not deep enough to interpret the LAB. Therefore two end member LAB interpretations were used to produce corresponding member structural models.

5.1.3 End-Member Models:

1. **Moho-LAB model:** This model assumed LAB to be 100 km below the Moho and follow the same geometry as Moho across the study area. (Figure 11).
2. **Onshore-constrain model:** This model used onshore lithospheric thickness constrains from Shapiro et al. (2004) and Romanowicz & Yuan (2010). Based on thickness estimates provided in the two studies, average onshore lithosphere thickness in the northern segment is ca. 200 km and ca. 150 km in the southern segment i.e. onshore LAB depth in the northern and southern segment is ca. 200 km and ca.150 km respectively (since pre-rift basement is expose onshore). Lithospheric thickness decreases as we transition offshore due to the evidence of past sea-floor spreading in the study area i.e. due to extinct mid-oceanic ridge (e.g.: Dickie et al., 2011). Owing to lack of an offshore LAB constrain, LAB depth was considered to remain constant after reaching a depth of 100 km. (Figure x).

Both models were refined through an iterative process in order to produce one finalized model that can was used for the application of the 3D rheological module. This process involved LitMod3D modelling and is elaborated in the next part of data analysis: Verifying via geophysical-petrological modelling.

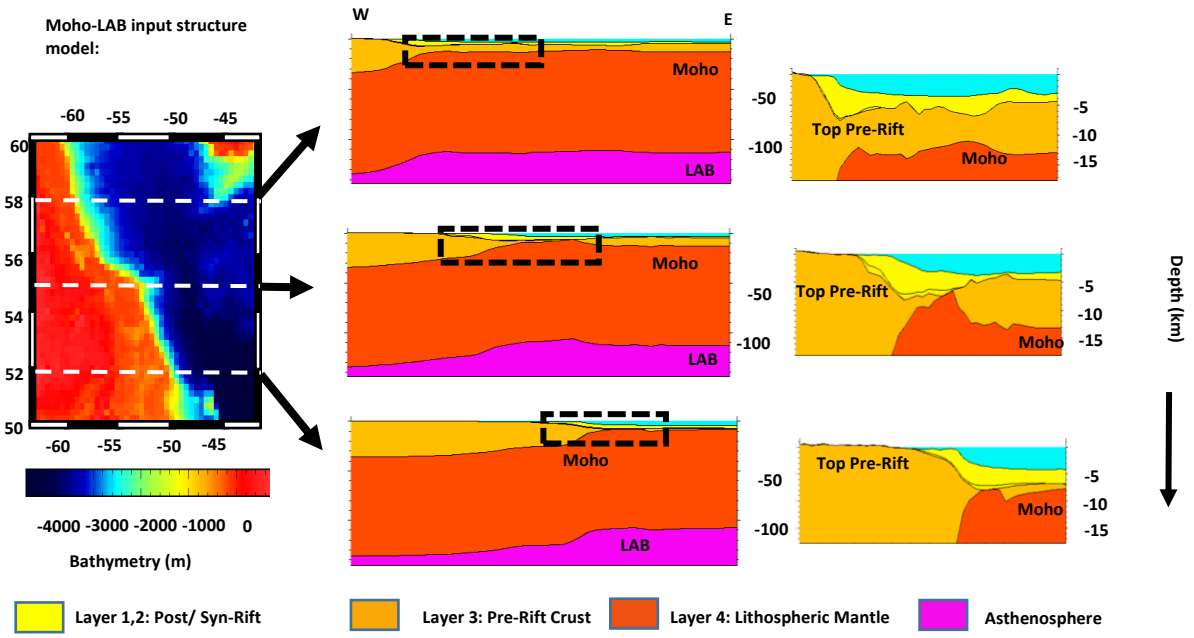

Figure 11: The input Moho-LAB structural model depicting lithosphere structure from north to south with constant lithospheric mantle thickness (100 km) across the study area.

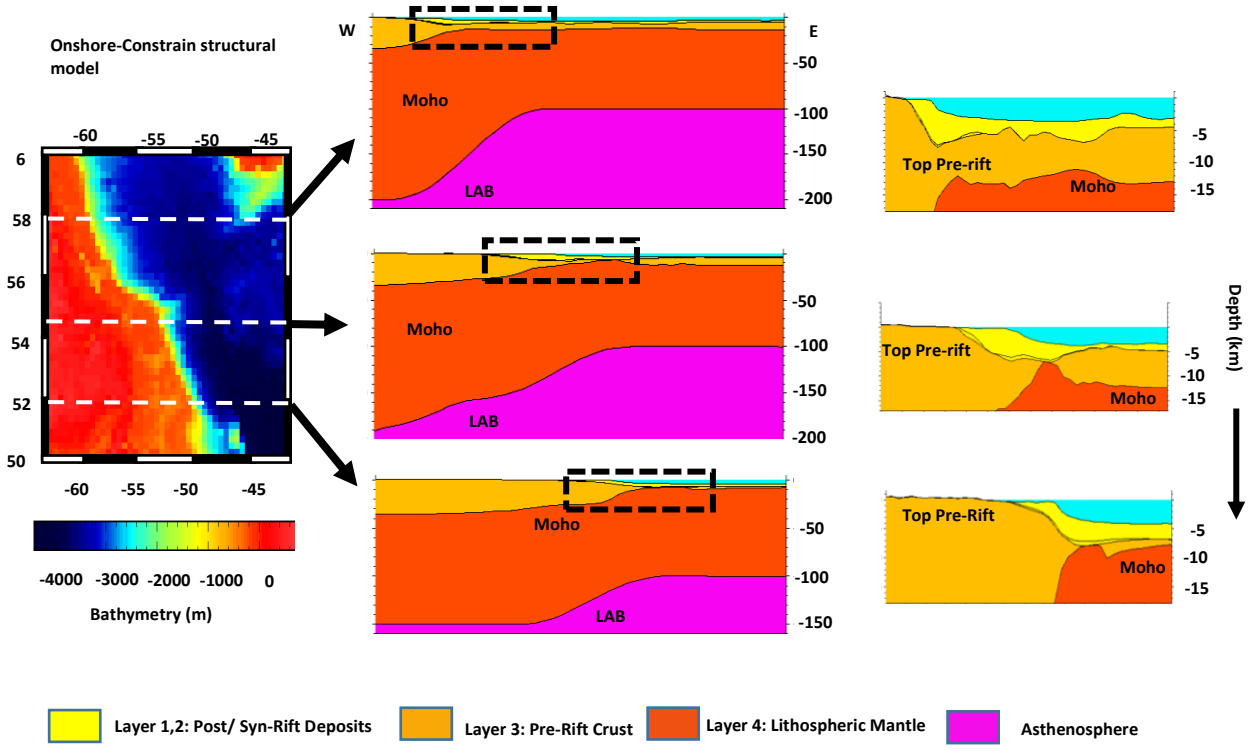

Figure 12: The input Onshore-Constrain structural model depicting lithosphere structure from north to south with higher lithosphere thickness in the onshore north compared to onshore south. Offshore mantle thickness stabilizes once it reaches a 100 km depth.

Composition of layers: Compositional parameters for both structural models were defined based on previous modelling attempts in the area (e.g.: GM-SYS profile modelling: Gouiza & Paton, in prep.) and lithological/mineralogical properties of the layers. The main parameters have been specified in Table 1.

No.	Layer	Dominant Lithology/ Mineralogy	Density (Kg/m^3)	Thermal Conductivity (W/mK)
1	Post-Rift deposits	Shale	2300	2.1
2	Syn-Rift deposits	Sandstone/Shale	2450	2.8
3	Pre- Rift crust	Variable	2850	3.0
4	Lithospheric Mantle	Olivine	3300	5.3

Table 1: Compositional variables of interpreted layers based derived from Gouiza & Paton (in prep.), Botter et al. (2017) and Eugene (1988).

5.2 Verifying via geophysical-petrological modelling

The end member structural models from the previous stage lacked proper data constrain for lithospheric structure. Both models were based on certain assumptions (as specified in the previous section) and required verification. This was done through residual maps as specified in section 4.2. The residual maps were divided into 9 subareas to explain mismatches observed in the study area. These are as follows:

1. North-western (NW) corner
2. Northern zone
3. North-eastern (NE) corner
4. Western zone
5. Central zone
6. Eastern zone
7. South-western (SW) corner
8. Southern zone
9. South-eastern (SE) corner

They have been specified in Figure 13. The objective was to find areas of good fit from both models and produce a lithosphere model that is best calibrated/ fitted to the observable data.

5.2.1 Moho-LAB model (ML):

This scenario has no data (complete assumption) constraint for the LAB depth. The major mismatches in the residual (calculated – observed) Geoid map lie in the NW, NE, SE and SW corners of the study area. The NW, SW and SE corners show negative differences of > ca. 20m and the NE corner shows positive differences of > ca. 20m. Another area of strong positive differences (ca. 15-20m) is present towards western and central zones the central zone. The rest of the study area shows a relatively decent fit with partial areas of northern and eastern zones showing large areas of negative mismatches (> ca. 20m) (Figure 13a,e)

Gravity anomalies show a similar areas of mismatch. Residual free air (FA) anomaly shows high differences in the corners of the study area. Partial parts in the NW and SW corners show large negative differences (> ca. 100 mgal). Areas in the NE corner show large positive differences (> 150 mgal), whereas the SE corner areas show large negative differences (> 100 mgal).The central and western zone shows a fairly strong positive differences (80 – 120mgals) (Figure 13b,f).

Bouguer anomaly also shows a similar tendency. Large negative differences (> 100 mgal) persist in the SW corner areas along with large positive differences for the NE corner (> 150 mgal). However Bouguer anomaly in the NW corner shows a decent fit (positive/ negative difference: 20-80 mgal). Residual Bouguer also shows fairly large positive differences (ca. 100-140 mgal) in parts of central, southern and western zones of the study area (Figure 13c.g).

The residual elevation shows difference between elevation calculated based on local isostasy principals (section2.3) and observed elevation. Large positive differences are observed in parts of SW, NW, SE corners and the western zone (> 1000m) along with strong negative differences in the parts of NE corner (> 1000m). Fairly large negative residuals are present in the central zone (ca. 480-500 m) of the study area. The rest of the study area mainly shows a fairly large positive difference (ca. 400 – 50m) with many parts in the NE corner, western and southern zone showing a fairly good match (positive/ negative differences: 0-30m) (Figure 13d,h).

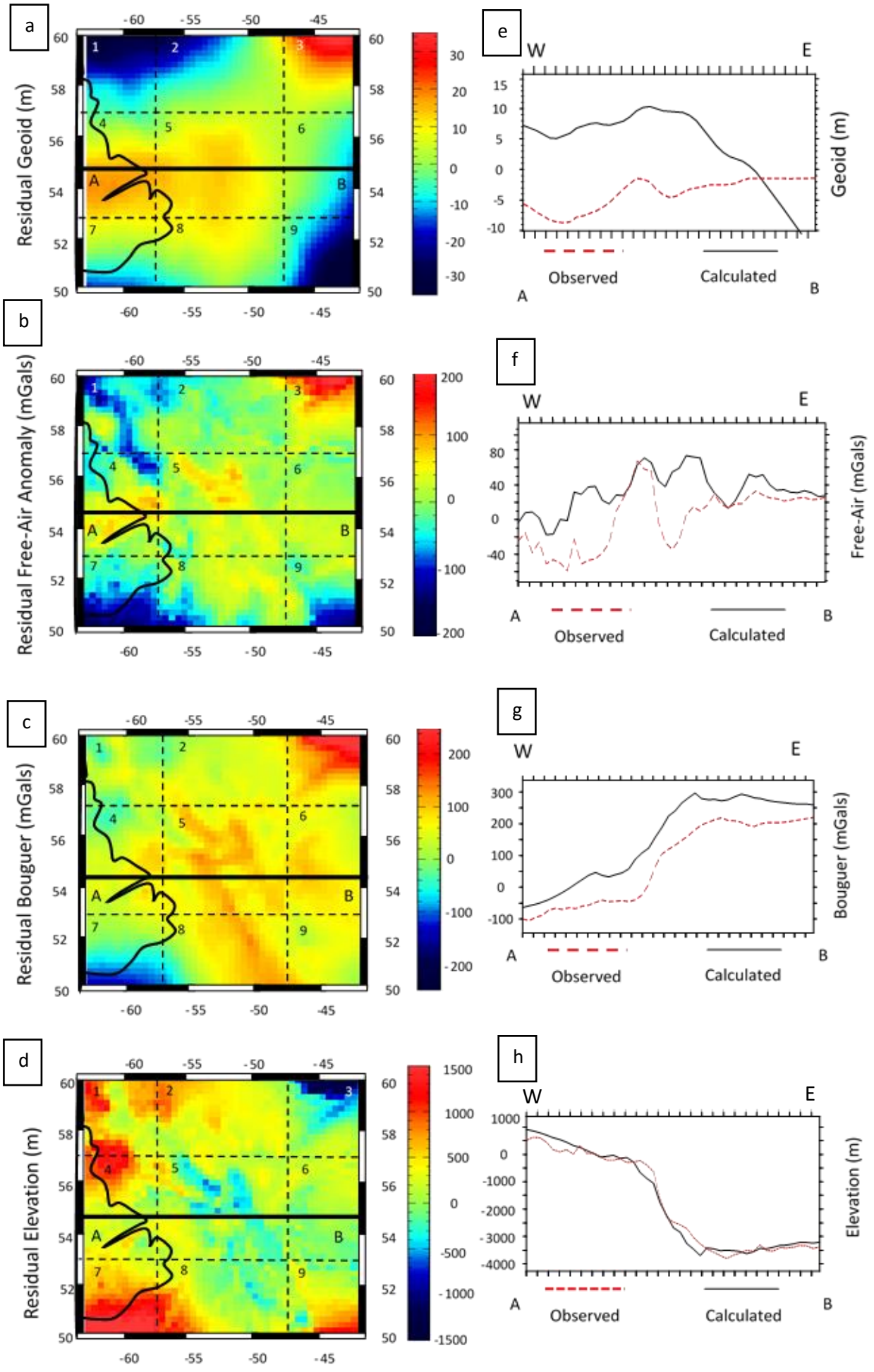

Figure 13: (a)-(d): Residual maps of Geoid, Free-Air, Bouguer and elevation for the Moho-LAB model highlighting the subareas (1-9) with cross-section line AB. **(e)-(h)** Cross-section view of line AB highlighting the difference between the observed and calculated geophysicals.

Onshore surface heat flow calculations show a relatively constant range from south to north (30 – 35 mW/m^2) with a sudden increments (> 35 mW/m^2) towards the extreme north (58°N and beyond) (Figure 14). Contrarily, observations from Mareschal & Jaupart (2004) indicate a depreciation of surface heatflow as we go from south to north

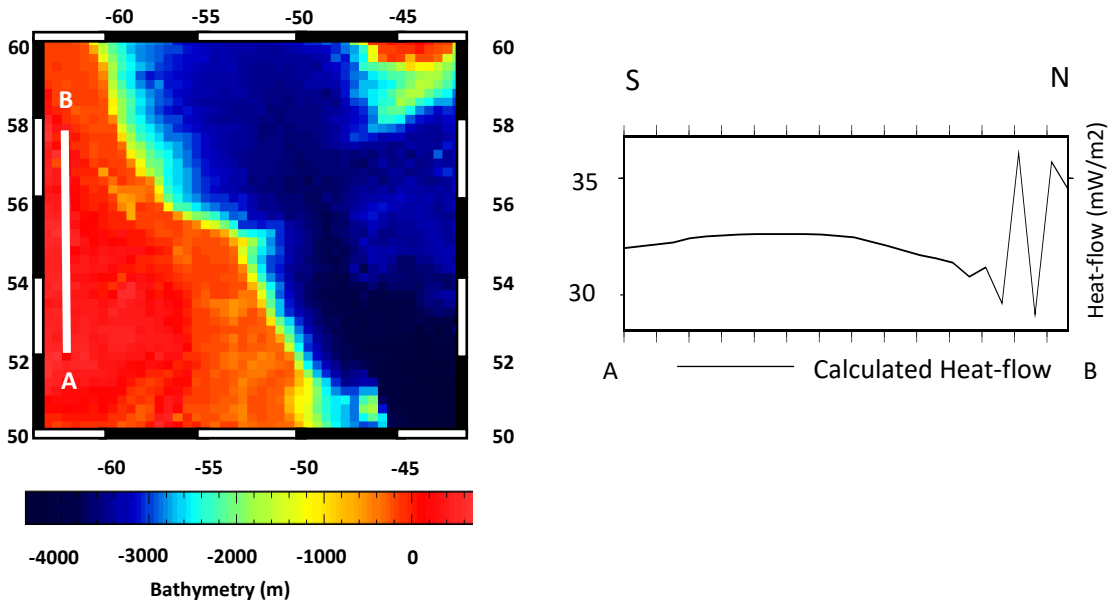

Figure 14: Surface heat-flow trend from north to south across the onshore Labrador lithosphere in the Moho-LAB model.

5.2.2 Onshore-constrain model (OC):

This scenario has partial data constraints (average onshore lithospheric thickness). Residual Geoid shows almost the same trend as the previous except for an in increase in area of large negative differences in the northern zone (> ca. 20m) and decrease of negative mismatch in the eastern zone (ca. 0m). Larger positive mismatches persist in the central and western zones (> 20m) (Figure 15a,e).

Residual FA indicates improved calibration for parts of NW corner as it shows minor positive/ negative differences (< ca. 20 mgal) in contrast to major negative differences from the previous model. Improvements are also seen in northern parts of the SW corner (ca. 51°N- 53°N) with smaller positive/ negative differences of 0-40 mgal (compared to >100 mgal from the previous model) but the strong negative differences for southern part (ca. 50°N- 51°N) of the SW corner persist along with large negative and positive differences in parts of NE and SE corners respectively. The western zone shows a large positive mismatch (ca. > 100mgals) compared to the previous model. Residual FA also shows a new area of fairly large negative mismatches (ca. 80-120 mgal) offshore towards the NE. This offshore area (Figure 15b,f) comprises of OD rocks and approximately coincides with the area where

oceanic accretion occurred due later stages of seafloor spreading (during Eocene: Figure 5).

Residual Bouguer shows large positive mismatches in parts of NW corner, central zone and the western zone (positive differences ca. 100-200 mgal). The NE corner area of large positive differences is smaller than the previous model. However, it shows improvements in the onshore parts of the SW corner (negative differences of < ca.100 mgal) compared to the previous model. Residual Bouguer for the aforementioned offshore NE zone (representing area of past seafloor spreading) improves (positive difference: ca. 0-30 mgal) and gives a better fit compared to the previous model (positive difference: 40-100 mgal) (Figure 15c,g).

Residual elevation shows improvement in some parts (minor negative differences: 20-40m) of the NW corner but is overcompensated in parts of the corner as areas of minor positive differences from the previous model turn to areas of large negative differences of ca. 500-1000m. A similar case exists for the western zone. Mismatch is observed in the NE offshore area (of past seafloor spreading) showing large positive differences (ca. 500-1000m). Positive elevation mismatches in the SW, SE corners remain the same. Negative mismatches in the central zone (ca. > 500) increase compared to the previous model. Overall there are more offshore areas of large mismatches compared to the previous model (Figure 15 d,h).

Onshore surface heatflow calculations indicate a decreasing trend from south to north which matches the trend suggested by Mareschal & Jaupart (2004). Going from south to north the average calculated heatflow in the Greenville, Makkovik and Nain/ Churchill provinces is ca. 30 mW/m^2, ca. 27 mW/m^2 and 25 mW/m^2 respectively. These values fall within the observed ranges of 27—47 mW/m^2, 27—37 mW/m^2 and 22—27 mW/m^2 for the three aforementioned provinces (in that order) (Figure 16).

5.2.3 Areas of best fit:

The onshore lithospheric structure from the onshore-constrain model was considered a better fit for observed data. Indeed, this is not reflected by the residuals, as both models present multiple onshore areas of large positive/ negative mismatch. However onshore surface heat flow north south trend roughly matched observed heatflow trend (section 3.2.3) as discussed by Gouiza & Paton (in prep.). Therefore onshore lithosphere structure for the onshore-LAB model was considered better constrained. Contrarily offshore lithosphere structure from the Moho-LAB model was deemed a better fit to the

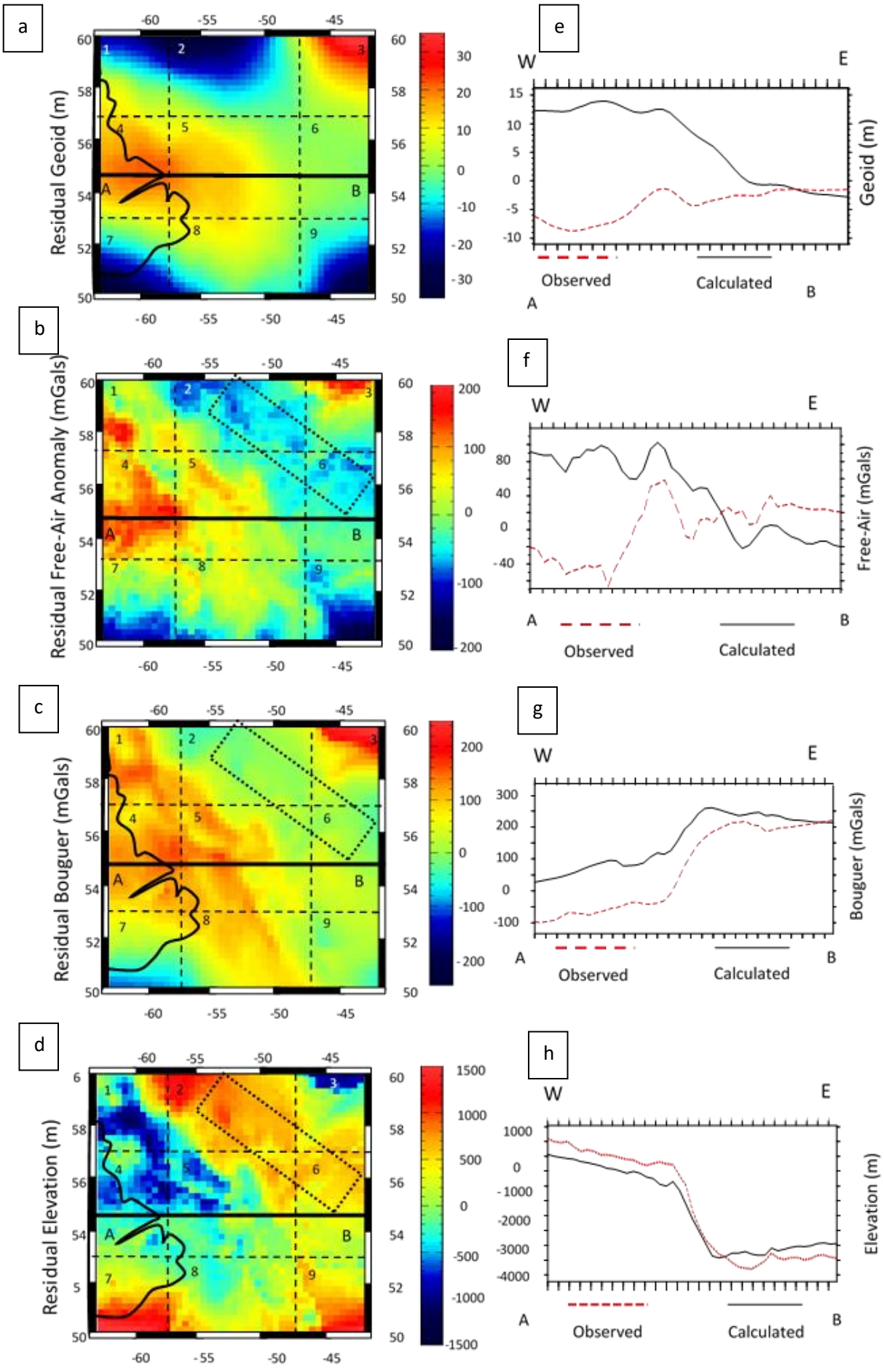

Figure 15: (a)-(d): Residual maps of Geoid, Free-Air, Bouguer and elevation for the Onshore-constrain model highlighting the subareas (1-9) with cross-section line AB and a dashed rectangle highlighting area of past seafloor spreading. **(e)-(h)** Cross-section view of line AB highlighting the difference between the observed and calculated geophysicals.

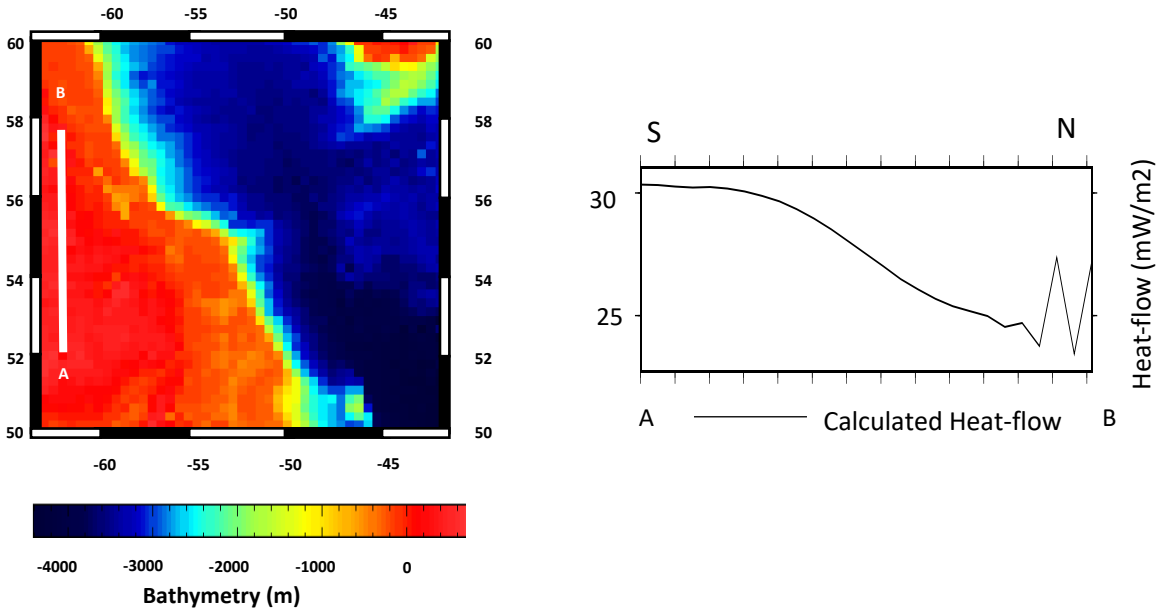

Figure 16: Surface heat-flow trend from north to south across the onshore Labrador lithosphere in the Onshore-Constrain model.

observables (although the lack of offshore LAB depth data constrain adds uncertainty). Therefore, by combining onshore lithosphere structure from the onshore-constrain model and with offshore structure of the Moho-LAB model, (i.e. combining areas of best fit from both models) a *principal model* was produced.

5.2.4 Adjustments:

The transition of LAB from onshore to offshore in the onshore-constrain model was adjusted such that offshore lithosphere structure from the Moho-LAB model was maintained as soon as LAB transitioned offshore (i.e. steeper LAB slope). Onshore lithospheric thickness was also increased towards the southern SW corner (ca. 170 km) to prevent a strong positive mismatch in the area (Figures 13-15). Figure 17 highlights the 3D structure of this model:

5.2.5 Principal Model:

Residual Geoid shows large negative differences in the NW and SE corners (> ca. 20m) along with a large positive difference (> ca. 20m) in the NE corner. The positive mismatch in the onshore western zone carries over from the OC model, but mismatch in central zone is reduced (ca. 6-12m) compared to the end-member models (ca. 12-14m)(Figure 18a,e).

Residual FA presents improvement (minor negative differences: ca. 20-60 mGal) in the offshore NE zone compared to onshore-lithospheric model. Positive differences (ca. 60-80 mgal) in parts of NW corner and western zone are smaller (60-100mGals) than the corresponding differences in the onshore-constrain model, but are larger than the Moho-

LAB model. Areas of large positive differences persist at the NE corner. Improvement compared to both models is observed in the onshore parts of the NW, SW corners and western zone (positive difference: 0-40 mGal). Similar improvement is also observed at the offshore central zone (positive difference: 40-80 mGal) and in the offshore SW corner (negative differences: 40-80m (Figure 18b,f).

Residual Bouguer shows improvements towards the NW corner (positive differences: 0-100 mgals) compared to the onshore-constrain model, but mismatches in some areas area are stronger than the Moho-LAB model. The NE offshore area depicts the opposite tendency as mismatches (20-60 mGals) are bigger than the onshore-constrain model (0-20mGals) but smaller compared to the Moho-LAB mode (60-60mGals). Improvements are observed for SW corner (negative difference: 60-80 mgal) compared to both models (negative difference: 80-120 mgal). Large positive mismatch areas in the NE corner (> ca. 100 mgal) and central zone are the same Moho-LAB model (Figure 18c,g).

Residual elevation in the NW corner and western zones still show some areas of overcompensation (minor positive to large negative differences) compared to the Moho-LAB model, but these are better constrained compared to the onshore-constrain model with average positive/ negative differences under ca. 500m. Negative differences in the central zone of the study area carry over from the Moho-LAB model. The onshore SW corner also shows a better fit (positive differences of ca. 0-80 m) compared to prior models but the offshore SW corner still has strong positive mismatches. The NE corner strong negative mismatch continues from the previous models. (Figure 18d,h)

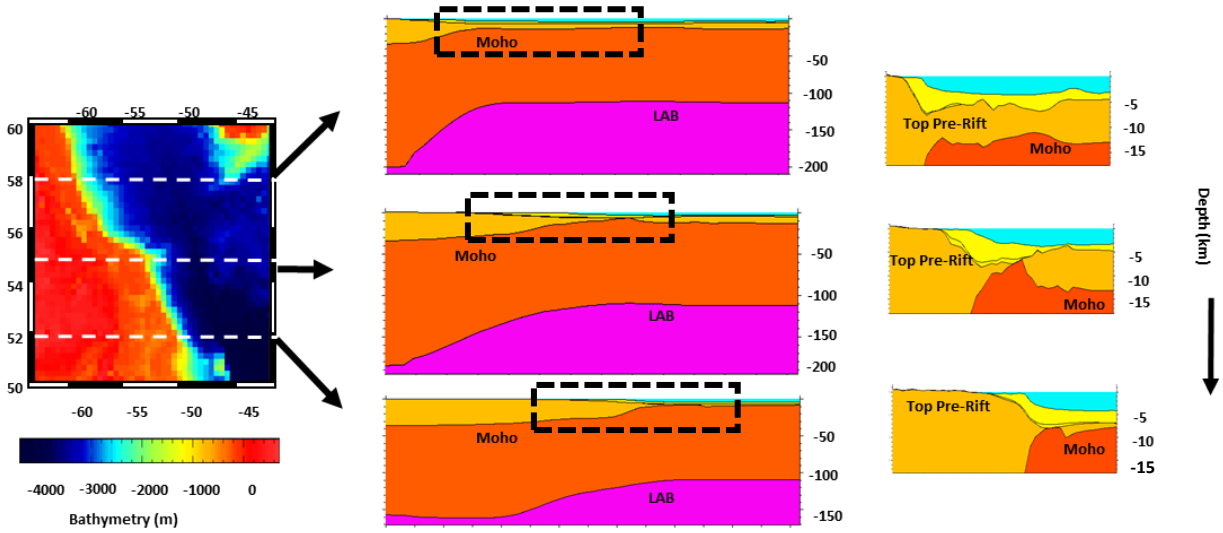

Figure 17: The Principal structural model depicting lithosphere structure from north to south with combined area of OC and MO models and a relatively steeper LAB slope

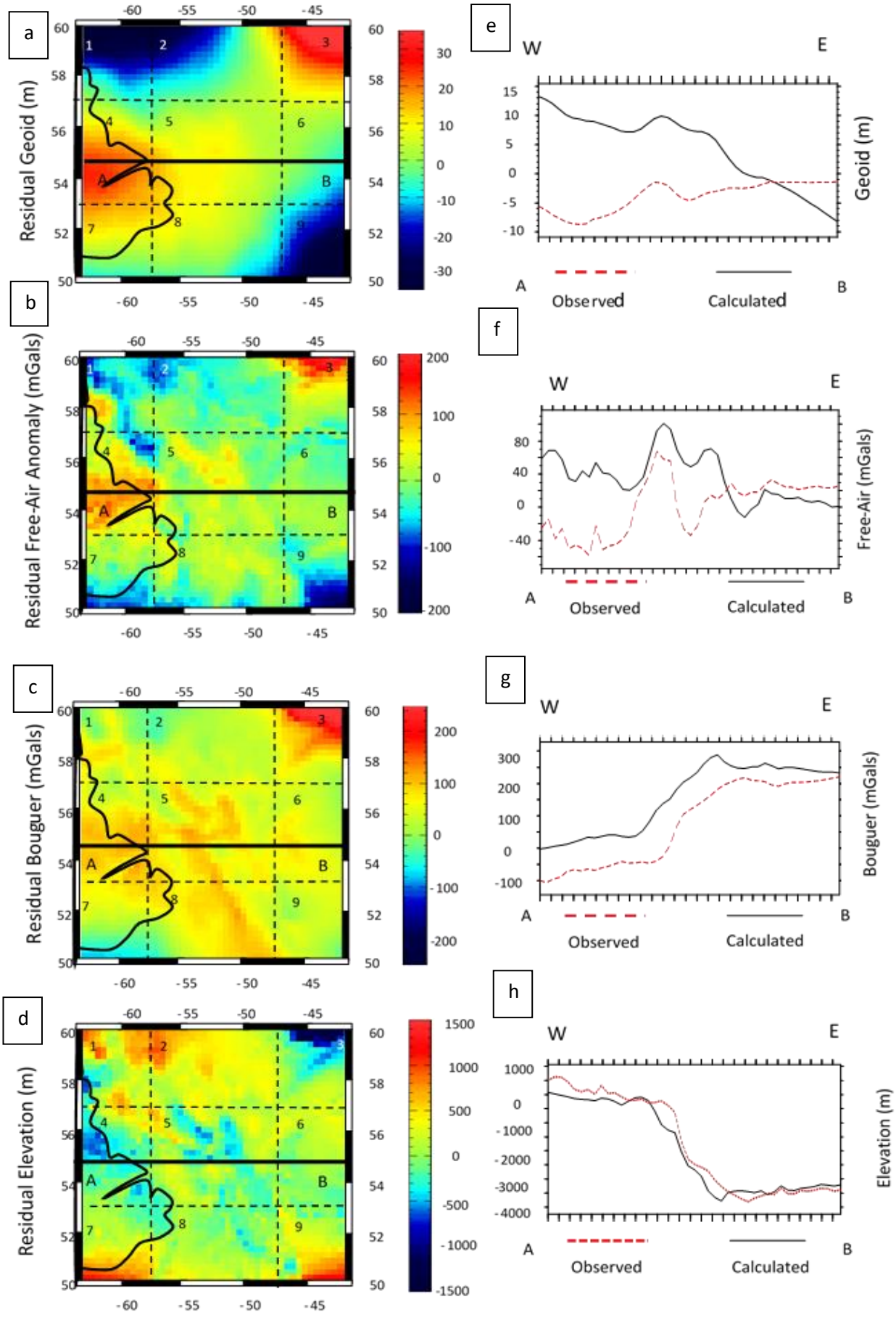

Figure 18: (a)-(d): Residual maps of Geoid, Free-Air, Bouguer and elevation for the Principal model highlighting the subareas (1-9) with cross-section line AB **(e)-(h)** Cross-section view of line AB highlighting the difference between the observed and calculated geophysicals.

Onshore surface heat flow calculations show a similar trend to the OC model except for lower heat-flow in the Greenville province (ca. 28 mW/m^2). Heat-flow towards extreme north again showed spiking towards the north (58°N and beyond) of ca. 30 mW/m^2 but the unexplained increment is larger compared to the OC model (ca. 27-28 mW/m^2) (Figure 19).

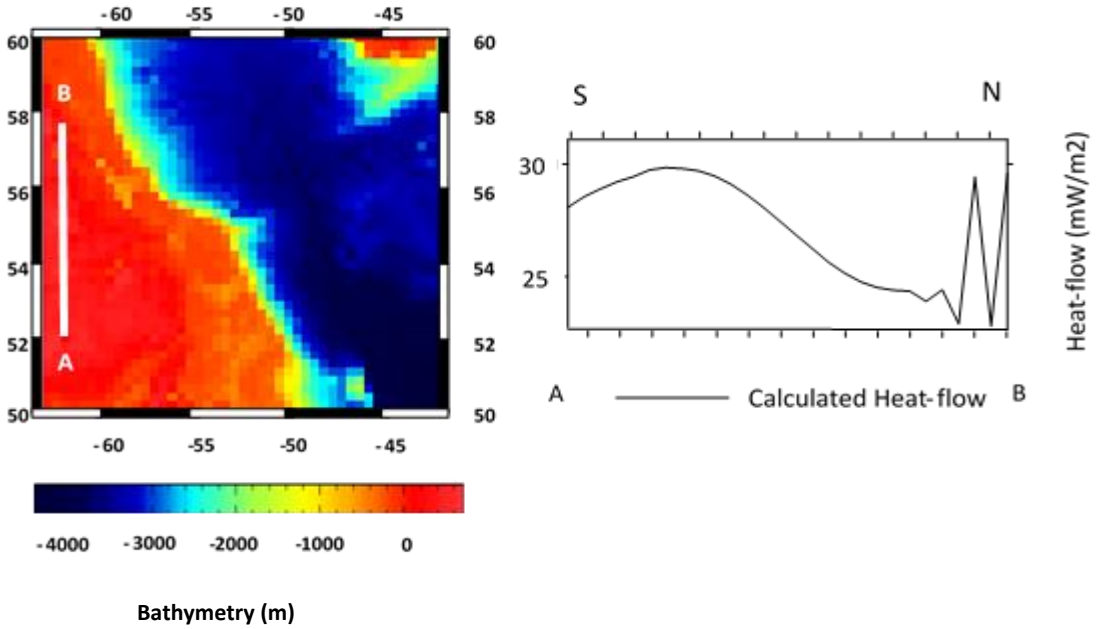

Figure 19: Surface heat-flow trend from north to south across the onshore Labrador lithosphere in the Principal model.

5.2.6 Persistent Differences:

Indeed the *principal model* does not give a completely accurate model of the lithosphere in the study area. Areas of residual mismatch in the study area are still present for this model. This can be attributed to the following

a) *Lack of lateral variability:* As mentioned in section 1, rifted margins can be divided into CD, TD and OD. The study area can be further divided into northern and southern segments that represent volcanic and non-volcanic margins respectively. The different domains in each of the segments are characterized by distinct physical properties including density (a crucial variable for the calculation of geoid/gravity anomalies and elevation) and thermal conductivity. However, models presented in this study assume the crust to be a single layer with homogenous properties across the study area. This idealization ignores variability of domains in both the segments (north/ south). Gouiza & Paton (in prep.) evaluated the crustal structure of the study area depicting lateral variability of crustal density in each domain. The integration of such lateral variability could constrain the models in a better way and could reduce mismatch in offshore areas such as the central zone and NE offshore

zones (that represent TD and OD in the southern and northern segments respectively). (Figure 10).

b) *Limited Data / Time:* Some parts of the study area show geophysical residual mismatch in all aforementioned models such as the NE/ SE corners. These corners are quite far away from the seismic lines on which the surfaces/ layers were interpreted. The layers were extrapolated to these corners via petrel. There could be structures present in this area that are not accounted for due to such extrapolation.

Lack of detailed data also causes similar problems. Onshore lithosphere thickness constrains (northern segment- 200 km, southern segment- 150km) used in the OC and principal models have been averaged for large parts of the study area. This is an idealistic assumption that assumes constant LAB depth over large parts of the study area discounting any structural changes in such parts. This could be responsible for the onshore areas of overcompensation present in the latter two models and large mismatches in the SW corner.

Areas of complete/ detailed data gaps can be constrained (to some extent) through further iterations using LitMod3D. Each iteration can help refine the structure of LAB (and hence lithosphere) so that it takes major/ minor structural variabilities into account. This study proceeds forward with EET calculation using the *principal model* due to the time constrain for this project in order to produce a preliminary rheological model of the study area. This preliminary model can be further developed with the integration of lateral variabilities and structural refinement.

5.3 Generating an EET map of the study area:

Using the calculated 3D geotherm, density and load from the *principal model*, the 3D rheological module was applied to calculate variable EET across the study area. Three different EET models are proposed in order to test various rheological parameters (RP) i.e. different lithospheric composition for each EET model.

- **Felsic-Olivine Model (FO):** Felsic-wet quartz crust (RP: Gleason and Tullis, 1995) and wet olivine (RP: Chopra & Paterson, 1984) in the lithospheric mantle.
- **Felsic-Peridotite (FP):** Felsic-wet quartz crust (RP: Gleason and Tullis, 1995) and wet peridotite (RP: Ranalli, 1995) in the lithospheric mantle
- **Mafic-Olivine model (MO):** Mafic-granulite crust (RP: Wilks & Carter, 1990) and wet olivine (RP: Chopra & Paterson, 1984) in the lithospheric mantle

The composition dictates the power law creep parameters assigned to each layer. The strain rate is assumed to be 10^{-15} s^{-1} and angle of friction is ca. 30°. Figure 21 shows the 3 different EET models with the composition of the crust/ lithospheric mantle specified. The general tendencies across the three models for the calculated load and EET are similar.

Load Tendency: The 2D distribution of load across the study area for each model is identical due to it being derived from the residual elevation mismatch of the principal model (section 4.3). The central and western zones shows high positive load (20-40 MPa). The southern and eastern zones show areas of relatively high positive loading (0-20 MPa). The onshore SW corner shows relatively low loading values (0-10 MPa) with high negative loading occurring in the offshore SW corner (20-40 MPa). The NW corner shows a mixture of high positive and negative loading (ca. 20-40 MPa). The SE corner shows high positive and negative loading (ca. 20-40 MPa) whereas the NE corner shows really high positive loading (ca. > 40MPa) (Figure 20).

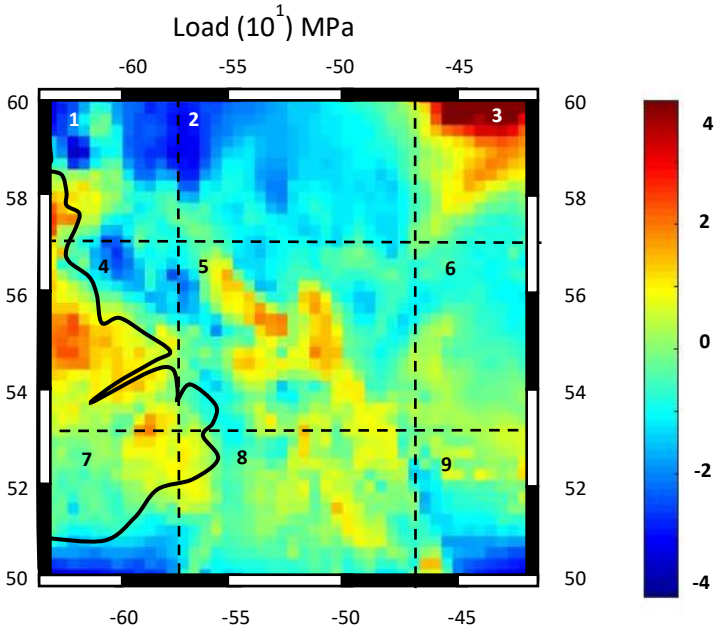

Figure 20: 2D Load distribution in the study area

General EET Tendency: Although EET values for the three cases are different its variation behaviour remains almost identical across the three different cases. EET in the central zone of the study area is quite low (FO, FP: ca. < 30km, MO: ca. < 45km, FA :). EET in the northern and southern zones is quite high (FO, FP: ca. 55-70km, MO: ca. > 70 km). A trend can be noticed in in the MO model where EET is fairly high in the NW corner (ca. 55-70km) and decreases as we go south into the western zone. The other two models show overall low EET values (ca. < 30km) in the corresponding area. This is followed by a rise in EET values towards the onshore part of the SW corner in all the models (FO, FP: ca. > 60km, MO: ca. >

70 km) and then diminishing EET values towards the offshore part of the SW corner. High EET values are noticed in the eastern zone (FO, FP: ca. 40-50km, MO: 50-70km).The NE and SE corners show low values in thee FO, FP models (20-40km) and a mixture of high and low values for the Mo model (ca. 30-70km). (Figure 21).

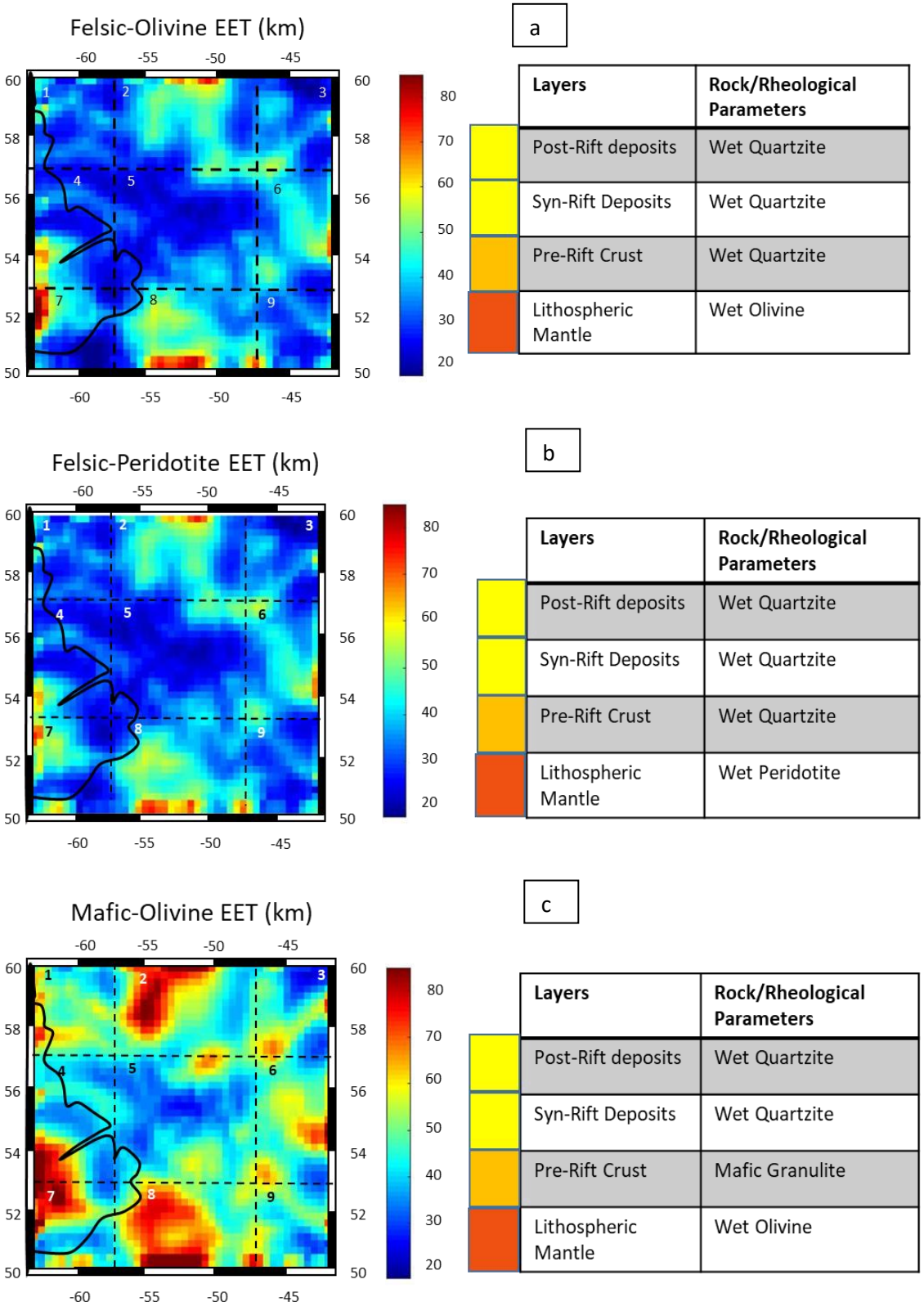

Figure 21: Laterally variable EET calculated using different crustal and mantle composition as highlighted in the tables (a): FO (b): FP and (c):MO.

6 Discussion:

Although calculated EET tendencies for the three models are quite similar, there is difference pertaining to the range of EET values. This difference can be attributed to the variance in crustal composition across the three models and geothermal gradient across the study area. If we consider the transition of rheological behaviour at the three different locations (YSE1, 2 and 3: Figure 22a) in the study area, the YSE at these locations in FO and MO models tell different stories. The FO model indicates the transition from brittle to ductile behaviour at an average depth range of ca. 50-70 km. The average differential stress for the brittle ductile transition is ca. 1000MPa (Figure 22b). Contrastingly in the MO model the average depth range for brittle to ductile transition is ca. 80-100km and the differential stress for this transition is ca. > 1000MPa (Figure 22b). Therefore, a correlation between crustal compositional properties and EET can certainly be inferred. Comparably, variance of mantle properties have a relatively minor effect on EET variations as indicated by the similarity in the EET map between the FO and FP models.

In terms of EET correlation, it is also important to consider heatflow and temperature distribution. LAB depth dictates regional heatflow and hence temperature distribution in the study area (e.g.: Mareschal & Jaupart, 2004). The temperature distribution indeed has an impact on the transition depth of rheological behaviour. As observed in Figure 22b,d, the transition from brittle to ductile behaviour occurs at shallow depths at YSE3. The LAB depth at this point is ca. 100-110 km (compared to LAB depth of ca. 200km and 150km at YSE1 and 2 respectively) and has a faster rate of temperature increase with depth (when compared with YSE1 and YSE2 geothermal curves). A lower differential stress is required to cause extension (or deformation in general) at such points compared to areas of lower thermal gradient (Figure 22b,d). This would also indicate onshore EET towards the south (YSE2) to be higher compared to the north (YSE1). Yet, onshore calculated EET seems to be increasing towards the south (Figure 21). Indeed the load has a bigger effect in dictating EET in this model. Specifically, the load in the southern onshore areas is calculated to be quite low compared to high loads in the northern onshore areas (e.g.: western zone: Figure 20). This effect of high loading is especially clear when the offshore areas of high loading (positive or negative) are compared to offshore areas on the EET map and a significant reduction in EET is observed (Figure20, 21). Offshore LAB depth on average relatively remains in a constant range of (100-110 km). The 3D temperature distribution in such an area is also relatively remains constant. Therefore, the offshore EET can be considered to be mainly dictated by loading in this model (similar to the onshore EET).

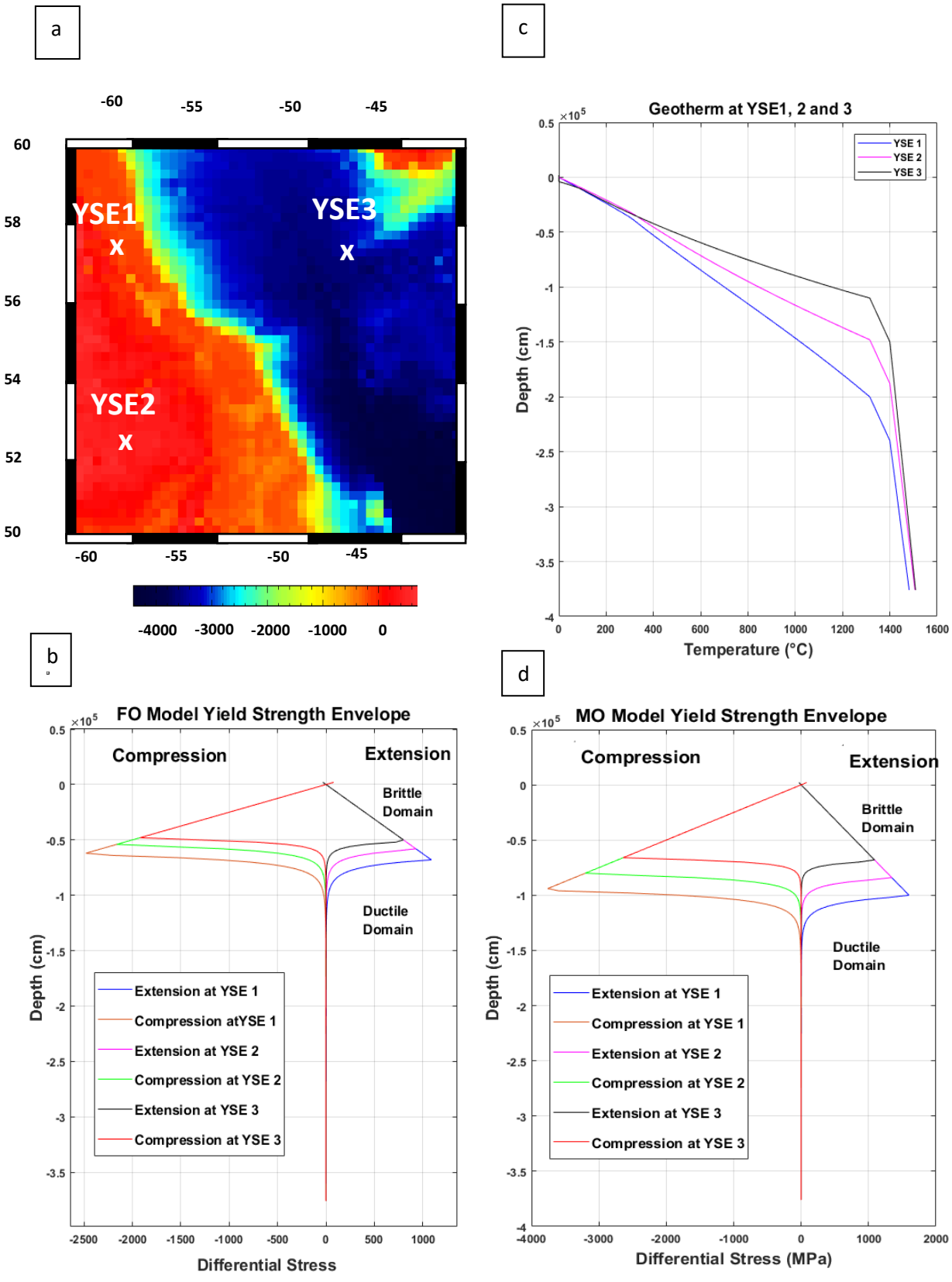

Figure 22: (a) Study area bathymetry showing points YSE1, 2 and 3 at which the YSEs have been derived. (b) FO model YSEs at the aforementioned points. (c) Geotherm (Temperature distribution) at the 3 different YSE points. (d) MO model YSEs at aforementioned points. YSEs calculated based on a Strain rate = 10^{-15} s^{-1} and angle of internal friction = ca. 30°

Hence crustal composition and loading (positive/ negative) are the two main factors controlling the lithospheric strength (EET) in this proposed lithosphere modelling process. Indeed these two factors on their own fail to highlight the explained north south asymmetry at the Labrador margin. However, there are some geological aspects that are not taken into account for this process. Primarily, the mechanical decoupling of the crust and mantle in areas of high heatflow. Previous studies have theorized that mechanical decoupling between the upper crust and upper mantle occurs in areas where the crust is thick enough (ca. 35km) and is accompanied with a high heatflow gradient (Burov & Diament, 1996). Such decoupling is thought to cause a higher reduction in EET. Indeed there are many extents in the study area where the aforementioned crustal thickness with high heatflow criteria can be met (especially onshore areas). Therefore to get a better idea of EET one must take the decoupling effect into account.

The rift history of the region has also been suggested to be driven by such mechanical decoupling. Gouiza & Paton (in prep.) suggested a gradual decoupling from the northern to southern segments (section 5.1.1). In fact the southern segment (Figure10) was considered to have a double decoupling effect due to the segregation of crust into a felsic upper crust and mafic lower crust. This caused a delay in the embrittlement of the crust as well as the coupling of the mantle and crust in this segment. Hence crustal thinning (accommodated by the necking zone) due to hyperextension was more enhanced in the southern segment compared to the northern segment.

Considering this information, it will be prudent to integrate lithospheric inheritance by differentiating the upper and lower crusts in the southern segment and take the decoupling mechanism between the crust and mantle and within the crust itself into account when calculating EET. Even though this study has taken a variable 3D geotherm and a fairly constrained lithosphere structure into account; these factors are not enough explain the observed asymmetry across the Labrador margin as the crustal composition seems to be varying across it (from north to south). Changes in crustal composition is key factor controlling lithospheric strength (highlighted by the difference of EET values between MO and FO models). A laterally/vertically variable crustal composition (i.e. variation in 3D) in the study area should highlight the asymmetry in a better way as opposed to assuming the crust to be a homogenous layers (laterally and vertically). The lateral change in crust should also take into account the variable crustal properties (such as density) of CD,TD and OD along with the decoupling effect towards the southern continental crust to better constrain the modelling process. Indeed a change in crustal

composition might change the lithospheric structure (from the LitMod3D verifying stage) and hence the load as well. Therefore further iterations of this modelling process need to be performed using laterally variable crustal composition to highlight the structural asymmetry at the Labrador margin through EET variations.

7 Conclusions:

a) Lithosphere rheology is an important factor when calculating lithospheric strength. Variable rheology across the lithosphere will lead to variable lithospheric strength (EET)

b) Modelling the lithosphere with observable geophysical data requires one to take its lateral variability in thermal and mechanical properties into account. Multiple iterations through the LitMod3D modelling process are required to refine the structure of the lithosphere.

c) The load, 3D temperature distribution and a mono-compositional crust are not enough to understand the structural asymmetry of the Labrador margin through EET. The effect of mechanical decoupling needs to be taken into account by considering a laterally and vertically variable crust in order to gain a better understanding of this relation.

d) Indeed, such changes in crustal composition could change the residual geophysical/ elevation data as well. Therefore multiple iterations of the modelling process suggested in this study need to be run in order to properly understand the structure and strength of the lithosphere lying underneath the Labrador basin.

References:

Afonso, J.C., Fernàndez, M., Ranalli, G., Griffin, W.L., Connolly, J.A.D., 2008. Integrated geophysical-petrological modeling of the lithosphere and sublithospheric upper mantle: Methodology and applications. Geochemistry, Geophys. Geosystems 9, n/a-n/a.

Audet, P., Bürgmann, R., 2011. Dominant role of tectonic inheritance in supercontinent cycles. Nat. Geosci. 4, 184–187.

Botter, C and Fullea, J., in preparation. Modelling of a laterally varying effective elastic thickness using an integrated thermodynamic, geophysical and rheological framework.

Botter, C., Prada, M., Fullea, J. 2017. Thermodynamic, geophysical and rheological modeling of the lithosphere underneath the North Atlantic Porcupine Basin (Ireland), EGU General Assembly, 20, p. 5216

Burov, E.B., Diament, M., 1995. The effective elastic thickness (T e) of continental lithosphere: What does it really mean? J. Geophys. Res. Solid Earth 100, 3905– 3927.

Burov, E., & Diament, M. 1996. Isostasy, equivalent elastic thickness, and inelastic rheology of continents and oceans. Geology, 24(5), p. 419-422.

Chian, D., Keen, C., Reid, I. and Louden, K.E., 1995a. Evolution of nonvolcanic rifted margins: New results from the conjugate margins of the Labrador Sea: Geology, 23, p. 589–592

Chian, D., Louden, K.E. and Reid, I., 1995b. Crustal structure of the Labrador Sea conjugate margin and implications for the formation of nonvolcanic continental margins: Journal of Geophysical Research: Solid Earth, 100, p. 24239–2425.

Chopra, P.N. and Paterson, M.S., 1984. The role of water in the deformation of dunite. Journal of Geophysical Research: Solid Earth, 89(B9), pp.7861-7876.

Dickie, K., Keen, C.E., Williams, G.L. and Dehler, S.A., 2011. Tectonostratigraphic evolution of the Labrador margin, Atlantic Canada: Marine and Petroleum Geology, 28, p. 1663–1675.

Fullea, J., Afonso, J.C., Connolly, J.A.D., Fernàndez, M., García-Castellanos, D., Zeyen, H., 2009. LitMod3D: An interactive 3-D software to model the thermal, compositional, density, seismological, and rheological structure of the lithosphere and sublithospheric upper mantle. Geochemistry, Geophys. 429 Geosystems 10, n/a-n/a.

Franke, D., 2013. Rifting, lithosphere breakup and volcanism: comparison of Magma-poor and volcanic rifted margins. Mar. Pet. Geol. 43, p. 63-87.

Geoffroy, L., Burov, E.B. and Werner, P., 2015. Volcanic passive margins: another way to break up continents: *Scientific Reports*, **5**, p. 14828.

Gleason, G.C. and Tullis, J., 1995. A flow law for dislocation creep of quartz aggregates determined with the molten salt cell: *Tectonophysics*, **247**, p. 1–23.

Gouiza, M., Paton, D. in prep. The role of inherited lithospheric heterogeneities in defining the crustal architecture of rifted margins and the magmatic budget during continental breakup.

Jaupart, C., Mareschal, J. C., Guilloufrottier, L. & Davaille, A. 1998. Heat flow and thickness of the lithosphere in the Canadian Shield. Journal of Geophysical Research, 103, p. 15269-15286.

Mareschal, J.C. and Jaupart, C., 2004. Variations of surface heat flow and lithospheric thermal structure beneath the North American craton: Earth and Planetary Science Letters, 223, p. 65–77.

Masini, E., Manatschal, G., Mohn, G. and Unternehr, P., 2012. Anatomy and tectono-sedimentary evolution of a rift-related detachment system: The example of the Err detachment (central Alps, SE Switzerland): *Geological Society of America Bulletin*, **124**, p. 1535–1551.

Mohn, G., Manatschal, G., Beltrando, M., Masini, E. and Kusznir, N., 2012. Necking of continental crust in magma-poor rifted margins: Evidence from the fossil Alpine Tethys margins: Tectonics, 31, p. TC1012.

Pérez-Gussinyé, M., Watts, A.B., 2005. The long-term strength of Europe and its implications for plate-forming processes. Nature 436, 381–384.

Péron-Pinvidic, G. and Manatschal, G., 2009. The final rifting evolution at deep magma-poor passive margins from Iberia-Newfoundland: a new point of view: International Journal of Earth Sciences, 98, p. 1581–1597.

Ranalli, G., 1995. Rheology of the Earth. Springer Science & Business Media.

Robertson, E.C., 1988. Experimental study of the strength of rocks. Geological Society of America Bulletin, 66(10), pp.1275-1314.

Romanowicz, B. and Yuan, H., 2010. Lithospheric layering in the North American craton: Nature, 466, p. 1063.

Ros Bernabeu, E., 2013. Lithospheric Modelling: Laterally Varying Elastic Thickness. MSc Thesis - Universidad Complutense de Madrid.

Shapiro, N.M., Ritzwoller, M.H., Mareschal, J.C. and Jaupart, C., 2004. Lithospheric structure of the Canadian Shield inferred from inversion of surface-wave dispersion with thermodynamic a priori constraints: Geological Society, London, Special Publications, 239, p. 175-194.

Soto, M., Morales, E., Veroslavsky, G., de Santa Ana, H., Ucha, N. and Rodríguez, P., 2011. The continental margin of Uruguay: Crustal architecture and segmentation: *Marine and Petroleum Geology*, **28**, p. 1676–1689.

Srivastava, S.P. and Roest, W.R., 1999. Extent of oceanic crust in the Labrador Sea: Marine and Petroleum Geology, 16, p. 65–84.

Suckro, S.K., Gohl, K., Funck, T., Heyde, I., Ehrhardt, A., Schreckenberger, B., Gerlings, J., Damm, V. and Jokat, W., 2012. The crustal structure of southern Baffin Bay: implications from a seismic refraction experiment: Geophysical Journal International, 190, p. 37–58.

Tappe, S., Foley, S.F., Stracke, A., Romer, R.L., Kjarsgaard, B.A., Heaman, L.M. and Joyce, N., 2007. Craton reactivation on the Labrador Sea margins: 40Ar/39Ar age and Sr–Nd–Hf–Pb isotope constraints from alkaline and carbonatite intrusives: Earth and Planetary Science Letters, 256, p. 433–454.

Turcotte, D.L. and Schubert, G., 2002. Geodynamics, 456 pp.

Wilks, K.R. and Carter, N.L., 1990. Rheology of some continental lower crustal rocks. Tectonophysics, 182(1-2), pp.57-77.